Comparison of earthquake strains over 10(2) and 10(4) year timescales: Insights into variability in the seismic cycle in the central Apennines, Italy

Comparison of earthquake strains over 10^2 and 10^4 year timescales: Insights into variability in the seismic cycle in the central Apennines, Italy

J. P. Faure Walker,[1] G. P. Roberts,[1] P. R. Sammonds,[1] and P. Cowie[2]

Received 16 March 2009; revised 26 March 2010; accepted 12 May 2010; published 23 October 2010.

[1] In order to study the existence of possible deficits or surpluses of geodetic and earthquake strain in the Lazio-Abruzzo region of the central Apennines compared to 15 ± 3 kyrs multi seismic cycle strain-rates, horizontal strain-rates are calculated in 5 km × 5 km and 20 km × 20 km grid squares using slip-vectors from striated faults and offsets of Late Pleistocene-Holocene landforms and sediments. Strain-rates calculated over 15 ± 3 kyrs within 5 km × 5 km grid squares vary from zero up to $2.34 \pm 0.54 \times 10^{-7}$ yr^{-1} and resolve variations in strain orientations and magnitudes along the strike of individual faults. Surface strain-rates over a time period of 15 ± 3 kyrs from 5 km × 5 km grid squares integrated over an area of 80 km × 160 km shows the horizontal strain-rate of the central Apennines is $1.18^{+0.12}_{-0.04} \times 10^{-8}$ yr^{-1} and $-1.83^{+3.80}_{-4.43} \times 10^{-10}$ yr^{-1} parallel and perpendicular to the regional principal strain direction (043°–223° ± 1°), associated with extension rates of $\leq 3.1^{+0.7}_{-0.4}$ mm yr^{-1} if calculated in 5 km × 80 km boxes crossing the strike of the central Apennines. These strain-rates are similar in direction to strain-rates calculated using geodesy (over 126 yrs, 11 yrs and 5 yrs) and seismic moment summation (over 700 yrs); however, the magnitude is about 2.6 × less over a comparable area. The 10^2 yr strain-rates are higher than 10^4 yr strain-rates in some smaller areas (≈2000 km^2, corresponding to polygons defined by geodesy campaigns and seismic moment summations) with the opposite situation in other areas where seismic moment release rates in large (>Ms 6.0) magnitude historical earthquakes have been reported to be as low as zero. This demonstrates the importance of comparing the exact same areas and that strain-rates vary spatially on the length scale of individual faults and on a timescale between 10^2 yr and 10^4 yr in the central Apennines. We use these results to produce a fault specific earthquake recurrence interval map and discuss the regional deformation related to plate boundary and sub-crustal forces, temporal earthquake clustering and the natural variability of the seismic cycle.

Citation: Faure Walker, J. P., G. P. Roberts, P. R. Sammonds, and P. Cowie (2010), Comparison of earthquake strains over 10^2 and 10^4 year timescales: Insights into variability in the seismic cycle in the central Apennines, Italy, *J. Geophys. Res.*, *115*, B10418, doi:10.1029/2009JB006462.

1. Introduction

[2] If strain calculated through seismic moment summation is less than that implied by geodetic measurements it may be that excess geodetic strain will be released in impending earthquakes. This approach has found favor in regions such as Greece and Italy because of its potential to identify the location and magnitude of future earthquakes [*Davies et al.*, 1997; *Clarke et al.*, 1998; *Hunstad et al.*, 2003]. However, uncertainty exists regarding the physical significance of such strain-rate comparisons and hence their interpretation.

[3] In this paper we suggest that comparison of strain-rates from seismic moment summation and Global Positioning System (GPS) measured over 10^2 yrs with longer-term strain-rates measured from geological offsets over 10^4 yrs or more will provide insights into the physical significance of geodetic and seismic strain comparisons. This is because evidence suggests that seismic cycles exhibit temporal variation, and such variation must be characterized before geodetic and seismic strains can be compared. For example, *Friedrich et al.* [2003], studying the Wasatch region of the U.S.A., show that strain-rates may be transient due to clustered strain release in earthquakes (~10 kyr) and post-seismic effects (10^2 yrs). Also, studies of displacement rates over 10^3–10^4 year timescales show that slip-rates on active faults stabilize when measured over time periods greater than 8000 years and less than 18000 years [*Bull et al.*, 2006; *Nicol et al.*, 2006]; at timescales less than 8000 years, strain-rates may be signifi-

[1] Research School of Earth Sciences, UCL/Birkbeck, London, UK.
[2] Institute of Geography, School of Geosciences, University of Edinburgh, Edinburgh, UK.

0148-0227/10/2009JB006462

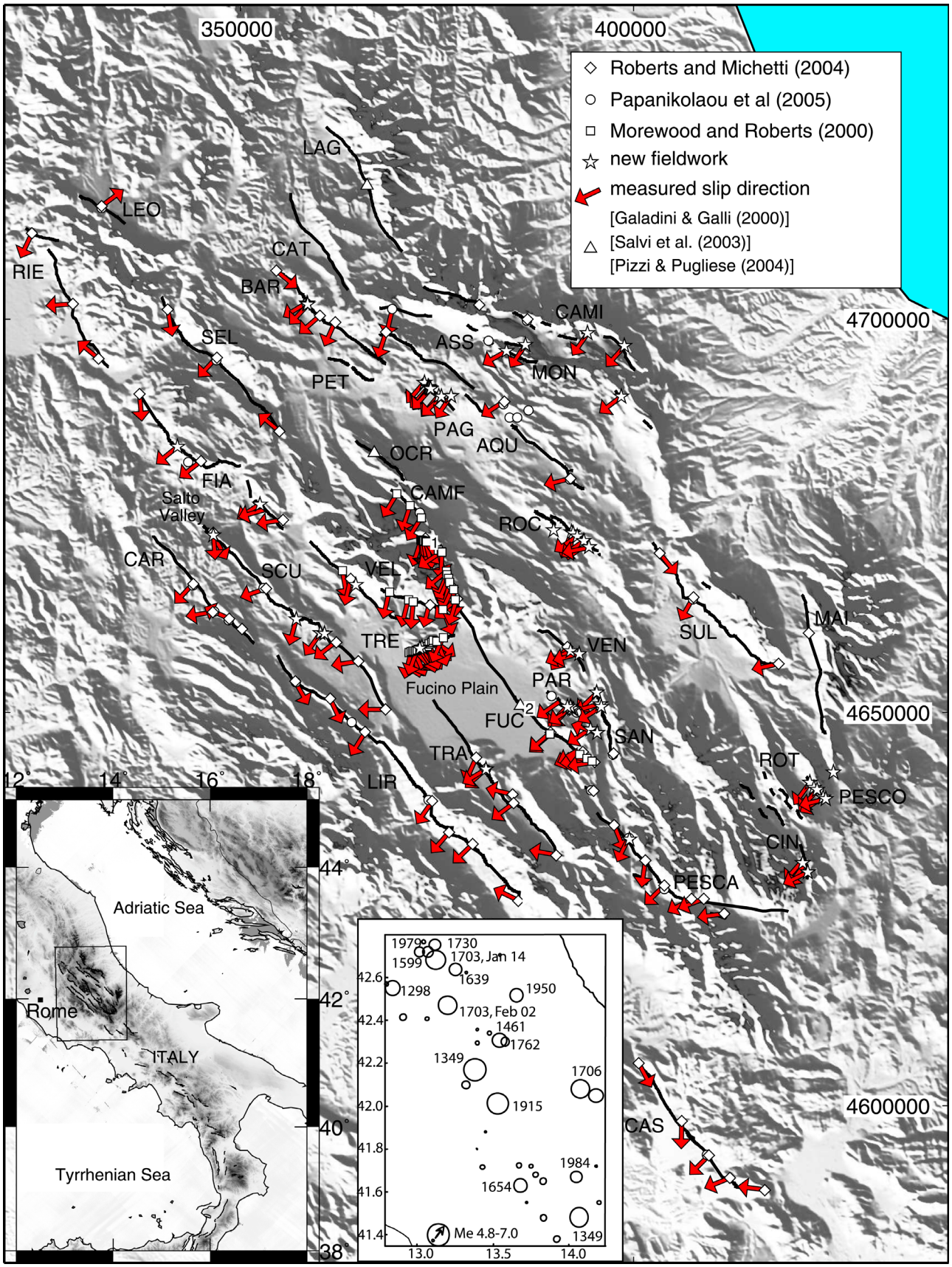
350000
400000
4700000
4650000
4600000
Roberts and Michetti (2004)
Papanikolaou et al (2005)
Morewood and Roberts (2000)
new fieldwork
measured slip direction
[Galadini & Galli (2000)]
[Salvi et al. (2003)]
[Pizzi & Pugliese (2004)]
LAG
LEO
RIE
CAT
BAR
SEL
PET
ASS
CAMI
MON
PAG
AQU
OCR
FIA
Salto Valley
CAMF
ROC
CAR
SCU
VEL
TRE
Fucino Plain
SUL
MAI
VEN
PAR
FUC
SAN
TRA
LIR
ROT
PESCO
CIN
PESCA
CAS
12°
14°
16°
18°
44°
42°
40°
38°
Adriatic Sea
Rome
ITALY
Tyrrhenian Sea
1979
1730
1599
1703, Jan 14
1639
1298
1950
1703, Feb 02
1461
1762
1349
1706
1915
1984
1654
1349
Me 4.8-7.0
42.6
42.4
42.2
42.0
41.8
41.6
41.4
13.0
13.5
14.0

Figure 1

cantly higher or lower than the true long-term strain-rate. It is thus desirable to gain a long-term strain-rate (in the order of 10^4 yrs) measured over multiple seismic cycles that allows one to gauge the significance of strain-rates measured over shorter timescales (in the order of 10^{1-2} yrs) and recognisee transients if they exist. Such long-term strain-rates should preferably be measured over length-scales short enough to identify individual active faults that may become the location of an impending earthquake. It is also essential that such measurements can be integrated over the exact same areas as those used for strain calculations from moment summations and the GPS, because strain is dependent on the length scales over which it is measured. To date, it has not been possible to directly compare geologic and shorter-term strain-rates, because (a) geologic strain-rates are known to vary along individual active faults with lengths as small as 20–30 km (for examples from Italy and Greece [*Morewood and Roberts*, 1999, 2000; *Roberts and Michetti*, 2004; *Roberts*, 2006]), (b) the spacings between geodetic stations are generally large (>30–50 km in Greece [*Davies et al.*, 1997], 60–70 km near Wasatch [*Friedrich et al.*, 2003], >30–60 km in central Italy [*Hunstad et al.*, 2003]), (c) the epicenters of large magnitude historical earthquakes for the last c. 1000 years are not known precisely and in many cases have not been assigned to individual active faults [e.g., *Selvaggi*, 1998], and (d) the directions of geologic strain-rate tensors are generally poorly constrained [see *Roberts*, 2006].

[4] This paper presents a new approach where long-term geologic strain-rates and strain directions are measured with high spatial resolution along a number of active normal faults in central Italy and integrated over the same areas as strain-rate measurements from geodesy and seismic moment summations. For these 20–30 km-long active faults, it is possible to measure (a) strain-rate magnitudes averaged over 15 ± 3 kyr from offset geology every few kilometers along the faults, and (b) strain-rate tensor orientations from kinematic data such as corrugated and striated fault planes from the same locations. We review existing measurements and present new data that together constrain the direction of slip at 155 sites from 7339 kinematic measurements, and the magnitudes of slip since 15 ± 3 kyr at 102 sites (Figures 1 and 2) [*Roberts and Michetti*, 2004; *Papanikolaou et al.*, 2005]. Shorter timescale strain-rates have been calculated using GPS geodesy velocities and summation of seismic moment release [*Selvaggi*, 1998; *Hunstad et al.*, 2003; *Anzidei et al.*, 2005; *Serpelloni et al.*, 2005]. The seismic moment release rates are facilitated by a historical record of large magnitude earthquakes that is thought to be complete since at least 1349 A.D. [*Michetti et al.*, 1996; *Valensise and Pantosti*, 2001], whilst interseismic deformation is constrained by campaign mode GPS networks, some of which re-occupy older triangulation networks, and permanent GPS stations. We add strains from the 6th April 2009 Ms 6.3 L'Aquila earthquake to the earthquake strains reported by *Selvaggi* [1998]. These combined data allow comparison of strain-rates over multiseismic cycles (15 ± 3 kyr, 10^4 yr), with those for time periods including single large magnitude earthquakes on individual faults (c. 700 years, 10^2 yr), and interseismic time periods (10^1–10^2 yr). These data from different timescales have not previously been compared in detail because of the problem of integrating strain over similar areas and a lack of information on the orientations of geological strain-rate tensors. Our grid approach allows us to compare strain-rates within polygons that have the same shapes and sizes as those used by seismologists and GPS geodesists. This is essential as strain-rates are dependent on the exact polygons shapes and sizes because different shapes and sizes have different lengths of active fault included within them and strain is dependent on the length-scale over which it is measured. The seismological strains of *Selvaggi* [1998] were computed by this author in triangular polygons; the geodetic strains of *Hunstad et al.* [2003] were computed in polygons of a variety of shapes set by the 126 year-old line-of-site triangulation survey that these authors re-occupied with GPS; using our grid we were able to compare these strains with our strains. Our method allows us to change the size and orientation of grid squares to match polygons from seismological and geodetic studies, a feature that had not been achieved prior to our study.

[5] It is important to compare long-term and short-term strain-rates for the central Apennines because it is well-known that strain-rates vary temporally and spatially, providing uncertainty regarding the physical significance of short-term measurements. For example, in the central Apennines, where spacings between published geodetic observations are c. 30–60 km [*Hunstad et al.*, 2003], recurrence intervals of >Ms 6.0 earthquakes measured in fault-trench investigations are in the range of 600 yrs to at least 3300 yrs [*Michetti et al.*, 1996; *Pantosti et al.*, 1996; *Galadini et al.*, 1997]. The Ovindoli-Pezza Fault has suffered 2 large magnitude earthquakes (>Ms 6.0) since 4.5 ka [*Pantosti et al.*, 1996], whereas, in a location only 18 km along strike (a distance shorter than the spacing of geodetic stations), at least 3 > Ms 6.0 earthquakes occurred

Figure 1. Map showing location of study area, mapped faults, measured slip directions and data collection sites where slip directions and/or scarp profiles have been measured. Also shown are sites from other authors from which data is used. The inset shows seismicity of the investigated area since 1200 AD taken from the working group CPTI [1999], adapted from *Galadini and Galli* [2000, Figure 1] (complete above magnitude 4.5 [*Vorobieva and Panza*, 2004]). AQU = L'Aquila Fault, ASS = Assergi Fault, BAR = Barete Fault, CAMF = Campo Felice Fault, CAMI = Campo Imperatore Fault, CAR = Carsoli Fault, CAS = Cassino Fault, CAT = Capitignano Fault, CIN = Cinque Miglia-Aremogna Fault, FIA = Fiamignano Fault, FUC = Fucino Fault, LEO = Leonessa Fault, LAG = Laga Fault, LIR = Liri Fault, MAI = Maiella Fault, MON = Monte Christo Fault, OCR = Ocre Fault, PAG = Paganica Fault, PAR = Parasano-Pescina Fault, PESCA = Pescasseroli Fault, PESCO = Pescocostanzo Fault, PET = Pettino Fault, RIE = Rieti Fault, ROC = Roccapreturo Fault, SAN = San Sebastiano Fault, SCU = Scurcola Fault, SEL = Sella di Corno Fault, TRA = Trassaco Fault, TRE = Tre Monti Fault, VEL = Velino-Magnola Fault, VEN = Ventrino Fault. 1. = Ovindoli-Pezza trench site [*Pantosti et al.*, 1996], 2. = San Benedetto di Marsi trench site [*Michetti et al.*, 1996].

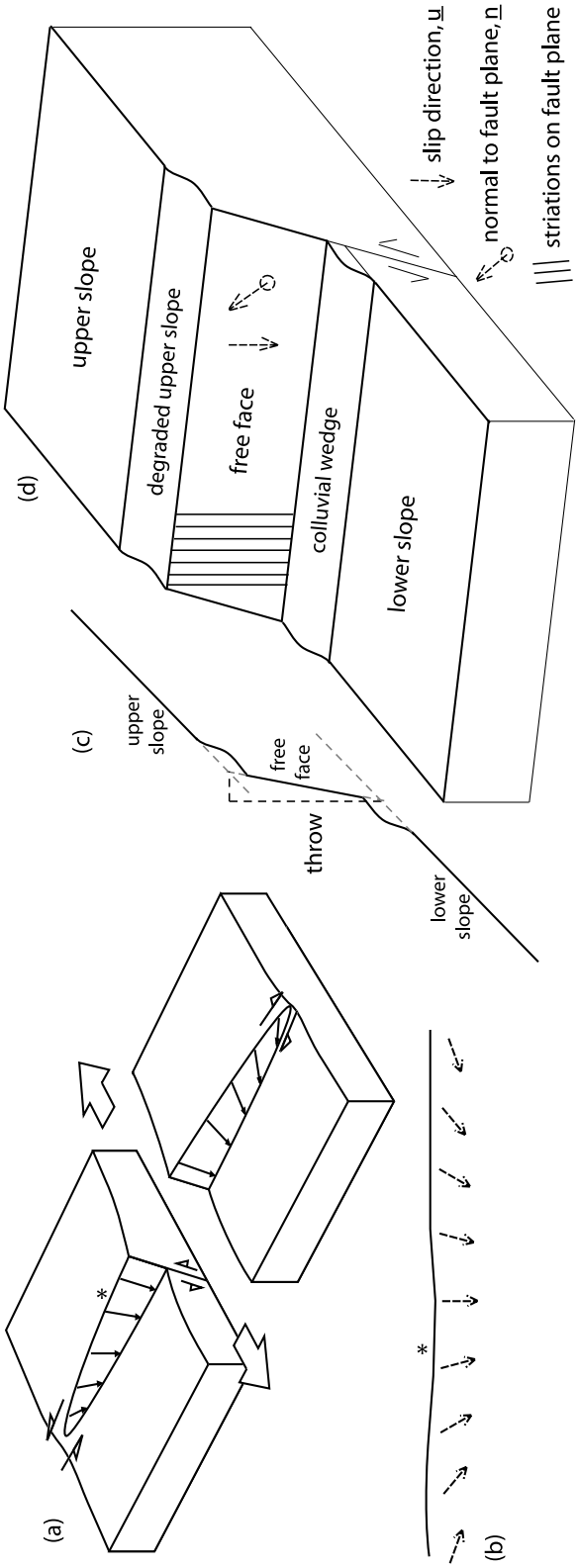

Figure 2. Cartoon of (a) change of throw and slip direction along fault (b) map view of slip directions along fault trace (c) scarp profile showing how throw is measured and (d) fault offsetting slope showing direction of slip vector and the normal to the fault plane at asterisk.

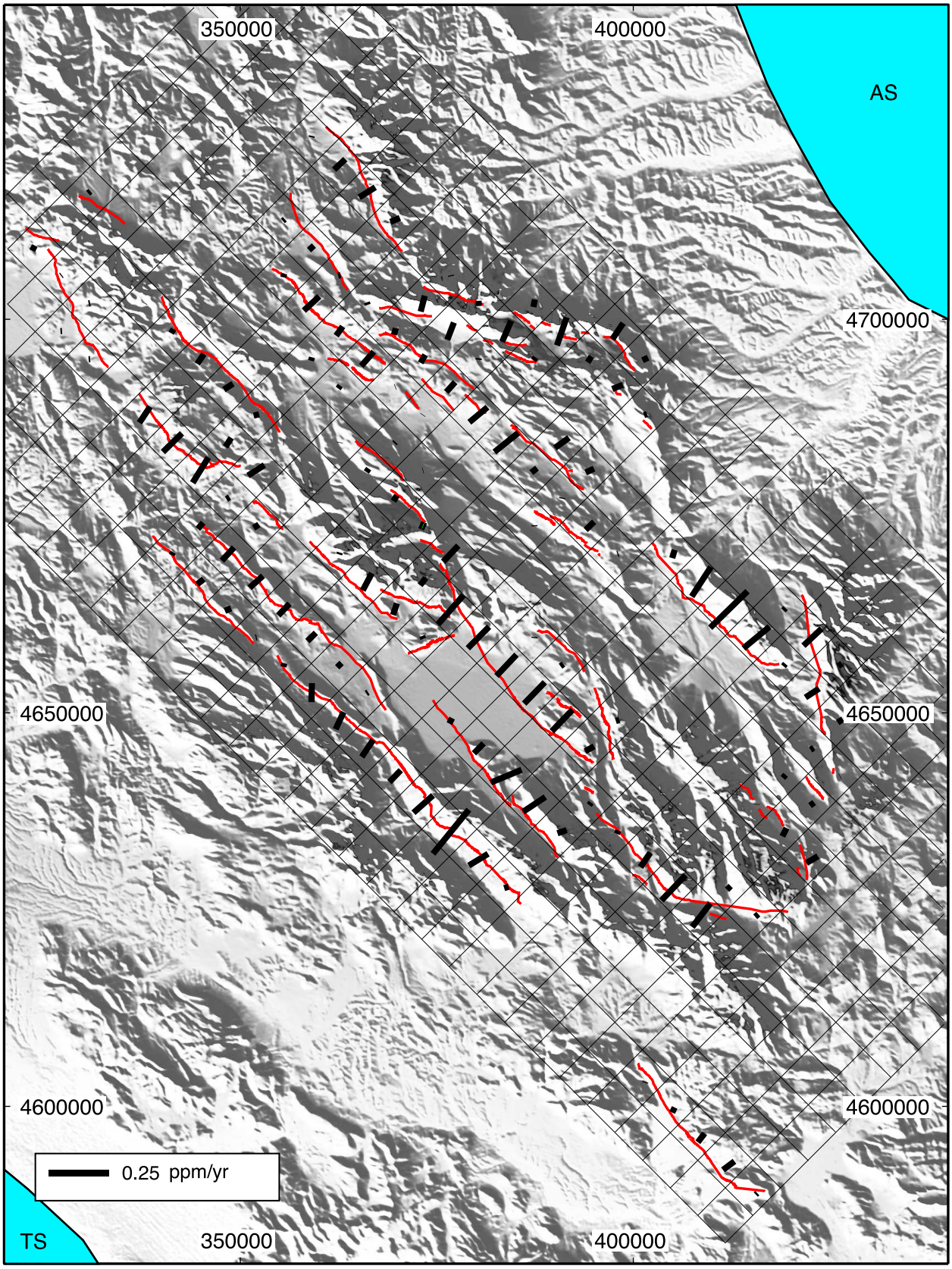

Figure 3. Average horizontal strain-rates in 5 km × 5 km areas shown in the orientation of maximum horizontal strain, calculated from measurements of striated faults offsetting Late Pleistocene and Holocene features. AS = Adriatic Sea, TS = Tyrrhenian Sea. Strain-rates perpendicular to those shown are too small to see at this scale (see Table 2).

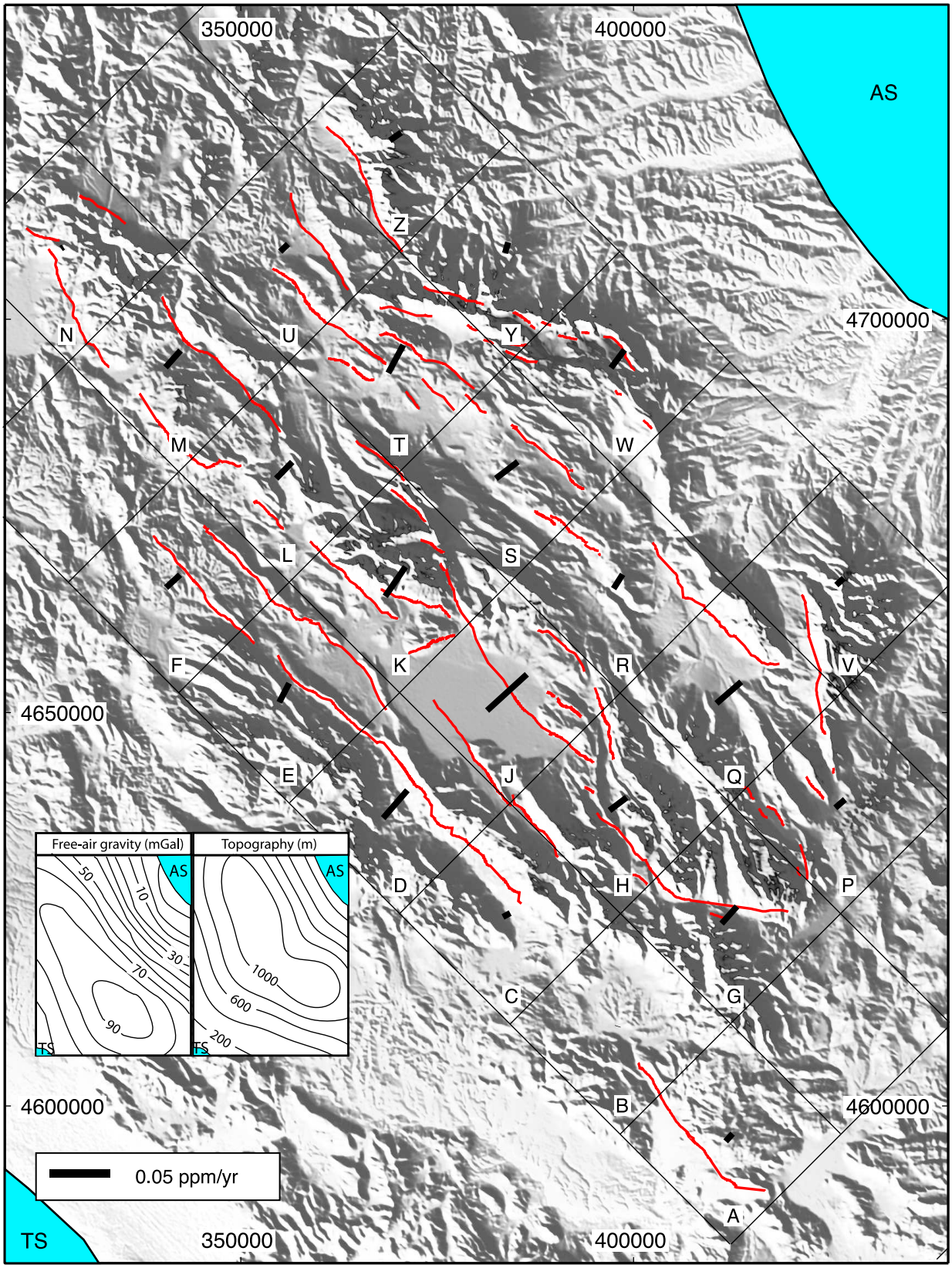

Figure 4. Average horizontal strain-rates in 20 km × 20 km areas shown in the orientation of maximum horizontal strain, calculated from measurements of striated faults offsetting Late Pleistocene and Holocene features. Also shown are the free-air gravity and topography maps for the same area [*D'Agostino et al.*, 2001b], AS = Adriatic Sea, TS = Tyrrhenian Sea. Strain-rates perpendicular to those shown are too small to see at this scale (see Table 3).

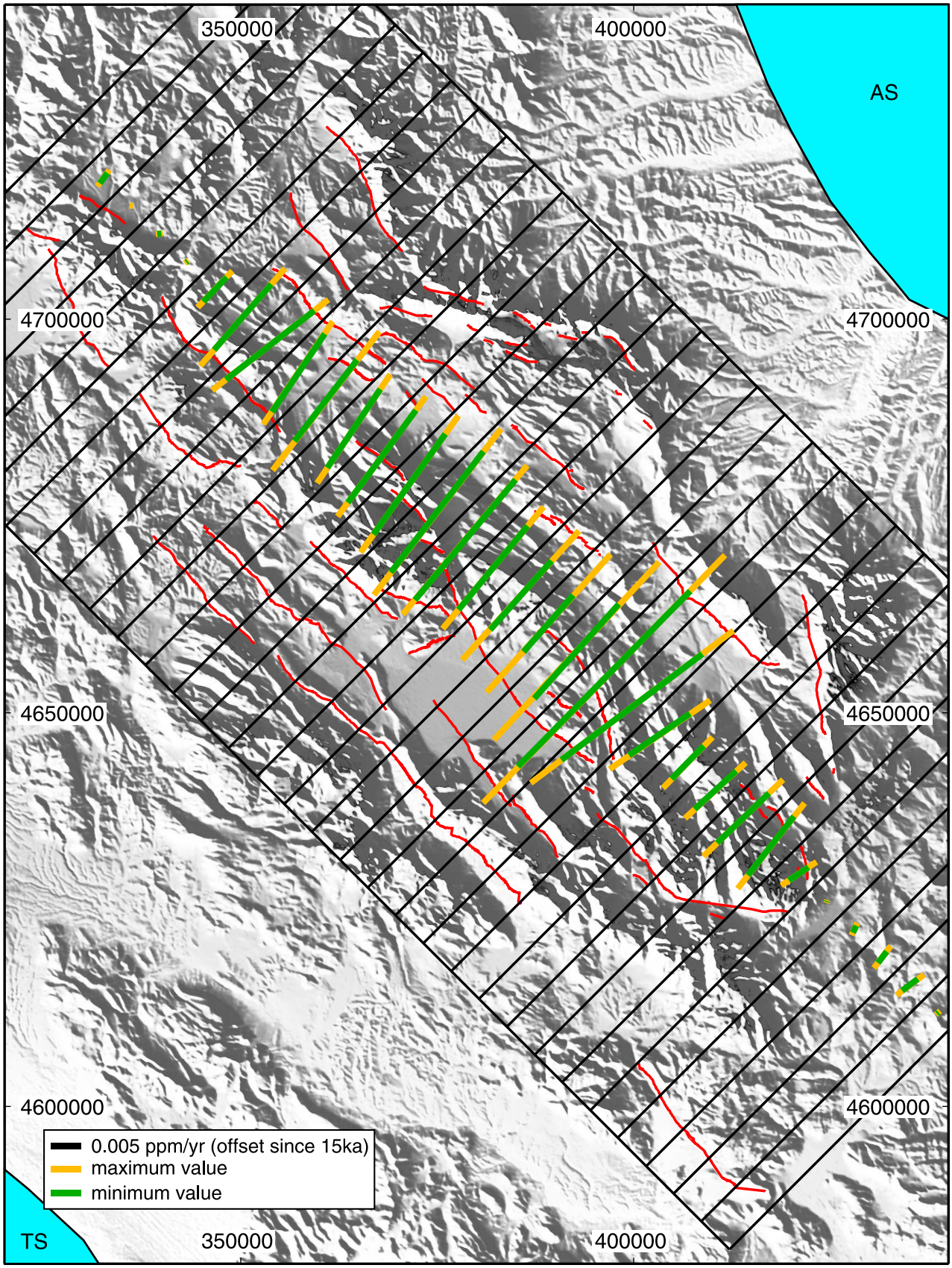

Figure 5. Principal horizontal strain-rates and extension rates along 5 km × 80 km transects across the Apennines calculated from offsets of Late Pleistocene-Holocene landforms showing how they change along the axis of the chain from NW to SE. AS = Adriatic Sea, TS = Tyrrhenian Sea.

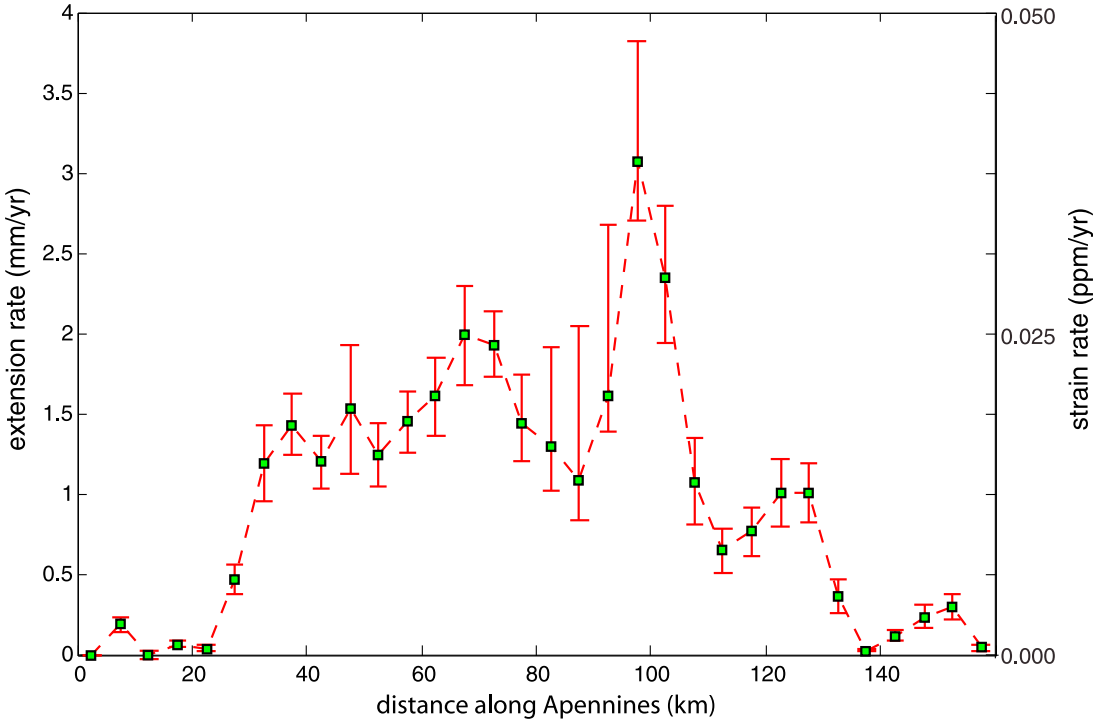

Figure 5. (continued)

on the San Benedetto dei Marsi Fault since c. 800 A.D. [*Michetti et al.*, 1996]. For the Velino-Magnola Fault, located only 7.5 km across strike from the Ovindoli-Pezza Fault, Cl^{36} cosmogenic exposure dating of surface slip events demonstrates temporal earthquake clustering on the Velino-Magnola Fault; 12 meters of surface slip accumulated in 0.5–3 m slip events (Mw 6.7–7.0) from 12 ka to 4.5 ka, with only one surface slip event since 4.5 ka [*Palumbo et al.*, 2004]. These spatial and temporal variations in the seismic cycle suggest that a measurement of strain at a high spatial resolution is needed. This must capture spatial variability at the length-scale of individual earthquake sources and over timescales including numerous seismic cycles to help judge the significance of short timescale deformation measured through seismic moment summations and Global Positioning System (GPS) geodesy. Specifically, we need measurements of deformation rates averaged over a time period long enough to include entire temporal earthquake clusters of large magnitude (>Ms 6.0) events, and the quiescent periods between them (anti-clusters) in order to constrain the rates of long-term loading on individual faults [*Main*, 1996]. We also need to know how such loading rates vary spatially across a system of active faults. This is because, if faults interact with each other, perhaps through stress transfer or fluid exchange [*Stein*, 2003; *Miller et al.*, 2004], an earthquake on one fault may produce transient changes in the deformation rates on neighboring faults [*Cowie*, 1998]. Ideally, we would like to know if measures of the short-term deformation from GPS geodesy and seismic moment summations record (a) transient effects related to earthquake interactions, (b) the long-term strain-rate, or (c) a combination of (a) and (b). Such findings would provide insights into the physical processes governing earthquake recurrence, improving our ability to

Figure 6. Map comparing the maximum principal strain-rates calculated using measurements of striated faults offsetting Late Pleistocene and Holocene features (green-yellow) with those calculated from summation of moment tensors over a time period of 700 years (purple-blue) [*Selvaggi*, 1998], with the addition of strains associated with the 6th April 2009 earthquake (Mw 6.3). The triangles show the apexes of the polygons used in the summation of moment tensors by *Selvaggi* [1998]; the drawn grid shows the areas used in this study. The mismatch between the grids is <3.5 km. AS = Adriatic Sea, TS = Tyrrhenian Sea, AQU = L'Aquila Fault, ASS = Assergi Fault, BAR = Barete Fault, CAMF = Campo Felice Fault, CAMI = Campo Imperatore Fault, CAR = Carsoli Fault, CAS = Cassino Fault, CAT = Capitignano Fault, CIN = Cinque Miglia-Aremogna Fault, FIA = Fiamignano Fault, FUC = Fucino Fault, LEO = Leonessa Fault, LAG = Laga Fault, LIR = Liri Fault, MAI = Maiella Fault, MON = Monte Christo Fault, OCR = Ocre Fault, PAR = Parasano-Pescina Fault, PESCA = Pescasseroli Fault, PESCO = Pescocostanzo Fault, PET = Pettino Fault, RIE = Rieti Fault, ROC = Roccapreturo Fault, SAN = San Sebastiano Fault, SCU = Scurcola Fault, SEL = Sella di Corno Fault, TRA = Trassaco Fault, TRE = Tre Monti Fault, VEL = Velino-Magnola Fault, VEN = Ventrino Fault. Note strain-rates perpendicular to the principal strain-rates were not calculated from the summation of moment tensors of historical earthquakes and hence are not shown for this study.

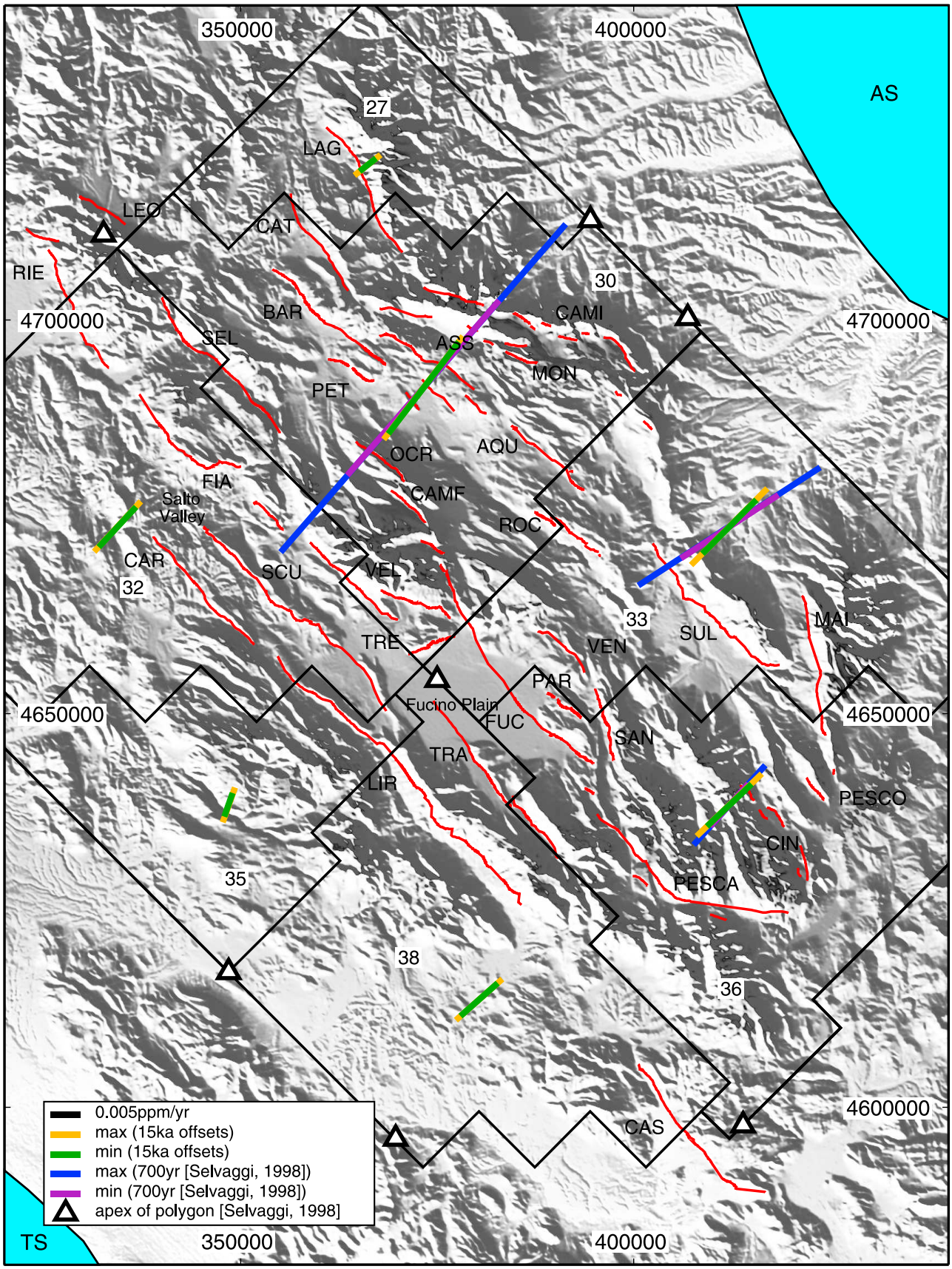
350000
400000
AS
27
LAG
LEO
CAT
RIE
30
4700000
BAR
CAMI
4700000
SEL
ASS
MON
PET
OCR
AQU
FIA
CAMF
Salto
Valley
ROC
CAR
SCU
VEL
32
33
MAI
TRE
VEN
SUL
PAR
Fucino Plain
4650000
FUC
4650000
SAN
TRA
LIR
PESCO
CIN
35
PESCA
38
36
4600000
CAS
0.005ppm/yr
max (15ka offsets)
min (15ka offsets)
max (700yr [Selvaggi, 1998])
min (700yr [Selvaggi, 1998])
apex of polygon [Selvaggi, 1998]
TS
350000
400000

Figure 6

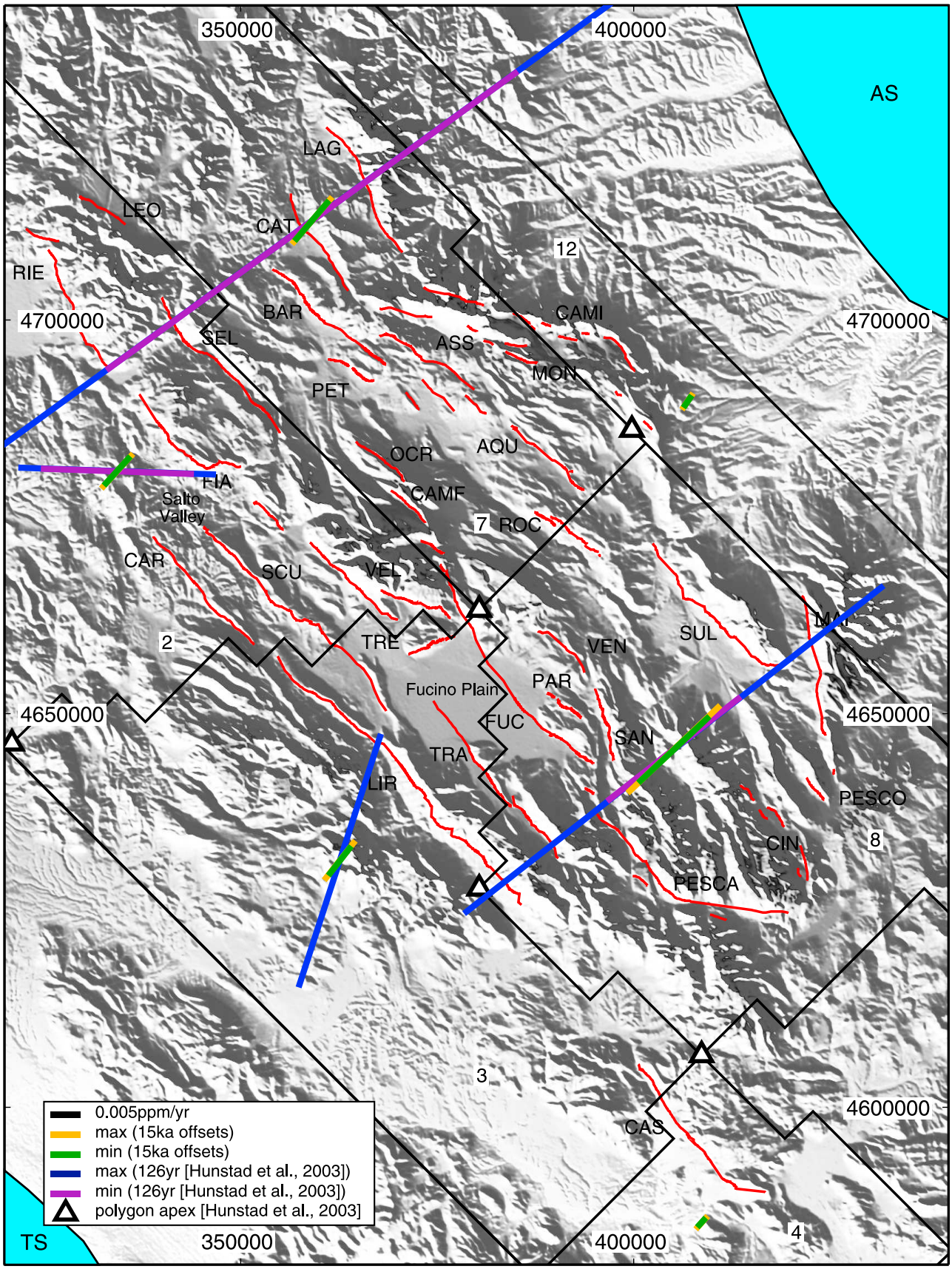
350000
400000
AS
LAG
LEO
CAT
12
RIE
4700000
BAR
CAMI
SEL
ASS
MON
PET
OCR
AQU
FIA
Salto
Valley
CAMF
7
ROC
CAR
SCU
VEL
2
TRE
VEN
SUL
MM
Fucino Plain
PAR
4650000
FUC
SAN
TRA
LIR
PESCO
8
CIN
PESCA
3
4600000
CAS
4
TS
0.005ppm/yr
max (15ka offsets)
min (15ka offsets)
max (126yr [Hunstad et al., 2003])
min (126yr [Hunstad et al., 2003])
polygon apex [Hunstad et al., 2003]

Figure 7

perform probabilistic seismic hazard assessments, and our understanding of continental deformation.

[6] In this paper we calculate 10^4 yr surface strain-rates from 12–18 kyr offsets across striated faults within 5 km × 5 km and 20 km × 20 km grid squares using adaptations of Kostrov summations [*Kostrov*, 1974] (Figures 3 and 4). We integrate these strain-rates (1) over 80 km × 5 km transects across the strike of the Apennines (Figure 5), (2) within comparable areas to 10^2 yr strain-rates implied by geodetic measurements and seismic moment summations (Figures 6 and 7) and, (3) over the 80 km × 160 km area to obtain a regional strain-rate. This allows us to compare strain-rates from 10^2 yr and 10^4 yr time intervals, and discuss variability in the seismic cycle and earthquake interactions. Our method is advantageous because it allows us to (1) calculate strain-rates over a time period that is long enough to include numerous seismic cycles on each fault, (2) calculate strain-rates at different length-scales and hence study how faults are interacting to produce regional strain-rates, and (3) compare strain-rates for varied polygon geometries imposed by the locations of GPS sites and seismic moment summations. We show that strain-rates vary between 10^2 yr and 10^4 yr timescales in the central Apennines *and* on a length-scale less than the length of individual faults (30–40 km). We use these results to produce a fault specific earthquake recurrence interval map (Figure 8) and discuss the regional deformation related to plate boundary and sub-crustal forces, the controls on the regional deformation, temporal earthquake clustering and the natural variability of the seismic cycle.

2. Geological Background and Deformation Rate Data

[7] Active extension in the Apennines occurs in previously shortened continental crust positioned within the zone of convergence between the Eurasian and African Plates [*Anderson and Jackson*, 1987; *Doglioni*, 1993]. Since the late Mesozoic, northward motion of the African plate has led to subduction of Tethyan ocean crust and collision of fragments of continental crust which now form the northern margins of the Mediterranean Sea, and the NW–SE striking fold-thrust belt in the Apennines. Thrusting continues to the present day on the Adriatic side of the Apennines, but, in general, NE-directed thrusting in central Italy ceased in the Pliocene [*Patacca et al.*, 1990]. Extension in the Apennines began at about 2.5–3.0 Ma [*Cavinato and De Celles*, 1999; *Roberts and Michetti*, 2004] with earlier extension to the west that produced thinned continental crust and ocean crust in the Tyrrhenian Sea. This extension eventually produced a volcanic province on the western coast of Italy. Extension may be due to a combination of roll-back of the Calabrian subduction zone [*Patacca et al.*, 1990; *Cavinato and De Celles*, 1999] and upwelling mantle [*D'Agostino et al.*, 2001b]. Focal mechanisms and borehole break-out data indicate active NE–SW extension concentrated along the main topographic ridge in central and southern Italy [*Anderson and Jackson*, 1987; *Pondrelli et al.*, 1995; *Montone et al.*, 1999], confirmed by studies of striated active normal faults at outcrop [*Michetti et al.*, 2000; *Roberts and Michetti*, 2004; *Roberts*, 2007]. The record of large magnitude earthquakes in the region spans over 1000 years with many written reports of damaging earthquakes that were most-likely normal faulting events located in the Apennines [*Postpischl*, 1985; *Boschi et al.*, 1995]; the record is thought to be complete since 1349 A.D. [*Michetti et al.*, 1996; *Valensise and Pantosti*, 2001]. The 1915 Fucino Earthquake (Ms 6.9–7.0) produced 15–20 km long surface ruptures that exhibited maximum co-seismic throws of about 1 m, and 33,000 fatalities [*Margottini and Screpanti*, 1998]. A magnitude 6.3 earthquake near the historical town of L'Aquila on the 6th April 2009 killed at least 287 people and made over 40,000 homeless (available at http://earthquake.usgs.gov/eqcenter/eqinthenews/2009/us2009fcaf/#summary).

[8] Scarps with striated and corrugated fault planes occur along the active normal faults, offsetting 12–18 ka landforms and sediments, allowing both the direction and rate of slip to be measured at numerous locations along each fault (Figure 2). The presence of moraines and glacial landforms reveals that the high topography of the Lazio–Abruzzo Apennines contained small (<10 km length) mountain valley glaciers during the last glaciation [*Giraudi and Frezzotti*, 1997], with periglacial conditions dominating most of the area which was not covered by ice. During the last glacial maximum, high erosion and sedimentation rates in periglacial areas outpaced fault throw rates evidenced by hanging wall fan surfaces and colluvial slopes associated with active faults that are graded to the slope of the footwall bedrock slope [*Roberts and Michetti*, 2004]. During the demise of the glaciation, the recovery of temperate vegetation stabilized the fan surfaces and mountain slopes reducing erosion and sedimentation rates. This allowed preservation of fault scarps produced by ongoing fault slip.

Figure 7. Map comparing the γ_1 shear strain-rates calculated using measurements of striated faults offsetting Late Pleistocene and Holocene features (green-yellow) with those calculated from GPS reoccupation of the first order triangulation network over a time period of 126 years (purple-blue) [*Hunstad et al.*, 2003]. The triangles show the apexes of the polygons used in the geodesy strain-rate calculations by *Hunstad et al.* [2003]; the drawn grid shows the areas used in this study. The mismatch between the grids is <3.5 km. AS = Adriatic Sea, TS = Tyrrhenian Sea, AQU = L'Aquila Fault, ASS = Assergi Fault, BAR = Barete Fault, CAMF = Campo Felice Fault, CAMI = Campo Imperatore Fault, CAR = Carsoli Fault, CAS = Cassino Fault, CAT = Capitignano Fault, CIN = Cinque Miglia-Aremogna Fault, FIA = Fiamignano Fault, FUC = Fucino Fault, LEO = Leonessa Fault, LAG = Laga Fault, LIR = Liri Fault, MAI = Maiella Fault, MON = Monte Christo Fault, OCR = Ocre Fault, PAR = Parasano-Pescina Fault, PESCA = Pescasseroli Fault, PESCO = Pescocostanzo Fault, PET = Pettino Fault, RIE = Rieti Fault, ROC = Roccapreturo Fault, SAN = San Sebastiano Fault, SCU = Scurcola Fault, SEL = Sella di Corno Fault, TRA = Trassaco Fault, TRE = Tre Monti Fault, VEL = Velino-Magnola Fault, VEN = Ventrino Fault. Note the strain-rates calculated from GPS for polygons 4 and 12 are not shown as they are compressional (see Table 5).

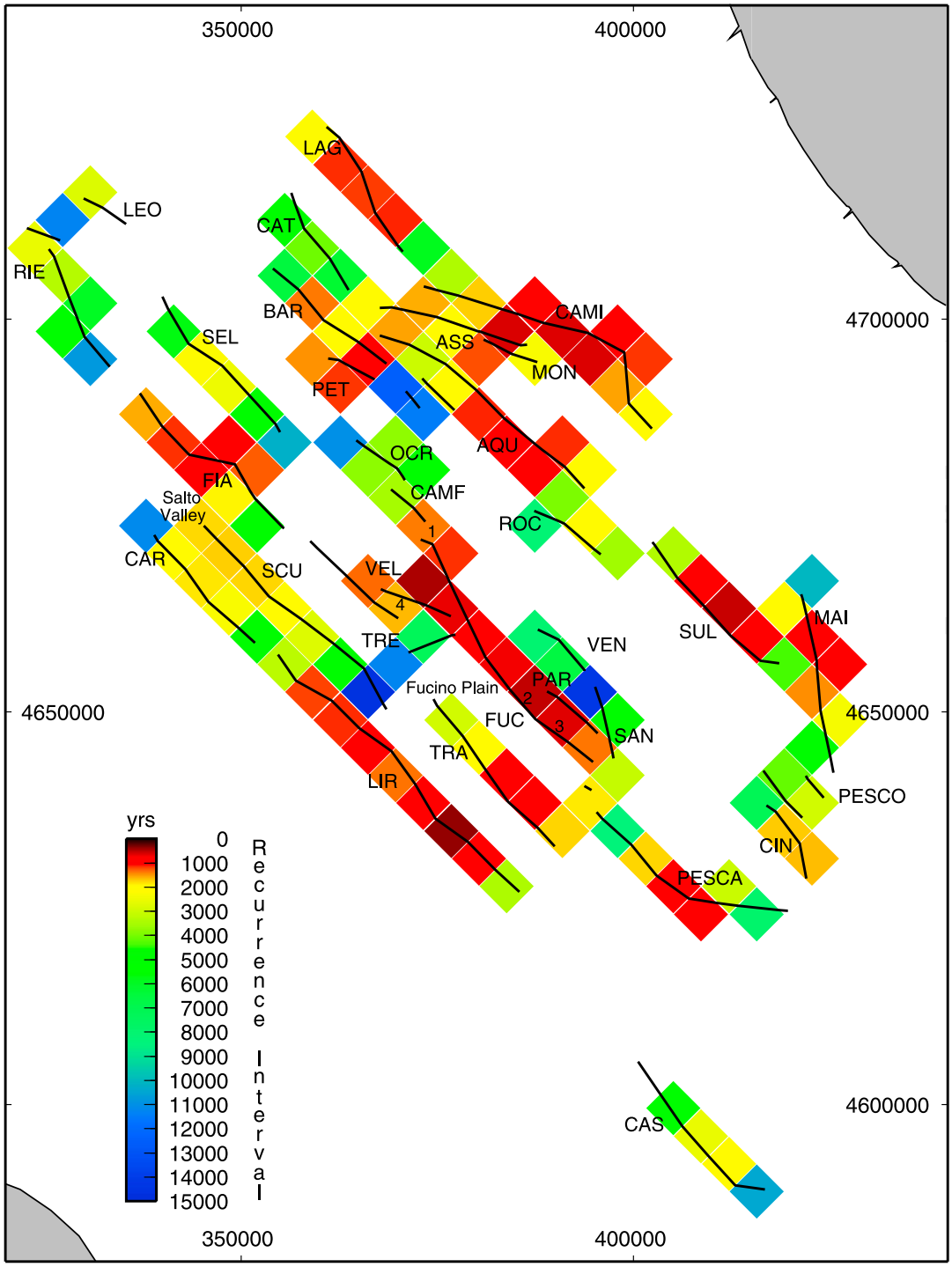

Figure 8. Map showing spatial distribution of earthquake recurrence intervals at a 5 km × 5 km resolution calculated from Late Pleistocene-Holocene offsets and assuming all earthquakes are dip-slip events with 1 m of slip. Grid squares containing discussed published paleoseismic observations are shown: 1, *Pantosti et al.* [1996]; 2, *Michetti et al.* [1996]; 3, *Galadini and Galli* [1999]; 4, *Palumbo et al.* [2004]. AQU = L'Aquila Fault, ASS = Assergi Fault, BAR = Barete Fault, CAMF = Campo Felice Fault, CAMI = Campo Imperatore Fault, CAR = Carsoli Fault, CAS = Cassino Fault, CAT = Capitignano Fault, CIN = Cinque Miglia-Aremogna Fault, FIA = Fiamignano Fault, FUC = Fucino Fault, LEO = Leonessa Fault, LAG = Laga Fault, LIR = Liri Fault, MAI = Maiella Fault, MON = Monte Christo Fault, OCR = Ocre Fault PAR = Parasano-Pescina Fault, PESCA = Pescasseroli Fault, PESCO = Pescocostanzo Fault, PET = Pettino Fault, RIE = Rieti Fault, ROC = Roccapreturo Fault, SAN = San Sebastiano Fault, SCU = Scurcola Fault, SEL = Sella di Corno Fault, TRA = Trassaco Fault, TRE = Tre Monti Fault, VEL = Velino-Magnola Fault, VEN = Ventrino Fault.

Table 1. Summary Table of Calculated Strain-Rates and Extension Rates Across the Central Apennines

Reference	Method	Time Period	Area (km^2)	Strain-Rate Across Apennines ($\times 10^{-8}$ yr^{-1})	Extension Rate (mm yr^{-1})
Serpelloni et al. [2005]	GPS	11 yrs	180 × 80	3.1 ± 0.8	2.5 ± 0.6
Anzidei et al. [2005]	GPS	4 yrs	180 × 130	1.4 ± 1.3	1.8 ± 1.7
D'Agostino et al. [2001a]	GPS	5 yrs	40 × 35	18 ± 3	6 ± 2
Hunstad et al. [2003]	GPS reoccupation of a triangulation network	126 yrs	various $\approx 10^3$	≤11	2.5 to 5
Selvaggi [1998]	Earthquake summation	700 yrs	various $\approx 10^3$	≤5.1 ± 1.5	1.6
Selvaggi [1998], with strain from the 2009 L'Aquila earthquake included	Earthquake summation	710 yrs	various $\approx 10^3$	≤5.5 ± 1.7	1.7
Roberts [2006]	Offsets of Late Pleistocene-Holocene sediments, 1-d summation of velocities	15 ± 3 kyr	64 (1d)	≤6.5 ± 1.5	≤4.3 ± 1.7
This study	Offsets of Late Pleistocene-Holocene sediments, Kostrov summation	15 ± 3 kyr	160 × 80	$1.18^{+0.12}_{-0.04}$	1.0 ± 0.1
This study	Offsets of Late Pleistocene-Holocene sediments, Kostrov summation	15 ± 3 kyr	various 5 × 80	$\leq 3.8^{+1.0}_{-0.5}$	$\leq 3.1^{+0.7}_{-0.4}$

[9] The chronology of the change from periglacial processes dominating slopes along active faults, to slopes controlled by surface slip and fault scarp growth processes is established by tephrachronology, Cl^{36} cosmogenic exposure dating and data on climate in the Mediterranean. Tephras from active volcanoes on the west coast of Italy cover the preserved periglacial slopes in the Apennines and several sites show that the slopes stabilized at about 18 ka [*Roberts and Michetti*, 2004, and references therein]. This is consistent with the fact that the last major glacial retreat phase occurred at c. 18–16 ka evidenced by a shift in $\delta^{18}O$ values from Tyrrhenian sea cores and cores from other marine areas [*Giraudi and Frezzotti*, 1986, 1997; *Allen et al.*, 1999]. Cl^{36} cosmogenic exposure dating has revealed that the fault planes associated with these scarps have formed since at least about 12 ka, and have grown incrementally through 1.5–3.0 meter slip events, probably associated with repeated Mw 6.7–7.0 earthquakes [*Palumbo et al.*, 2004, and references therein]. Erosion of the top of the fault plane, leaving an upper degraded slope, results in the top of the fault plane having a younger age than the offset. Hence the age of the top of the fault plane studied by *Palumbo et al.* [2004] gives a minimum age for the scarps (12 ka), whereas the climatic records and tephrachronology suggest they could be as old as 18 ka. In this paper we therefore assign an age of 15 ± 3 kyrs to the scarps to account for the uncertainty; this age is consistent with earlier papers [e.g., *Armijo et al.*, 1992; *Piccardi et al.*, 1999; *Roberts et al.*, 2002; *Roberts and Michetti*, 2004; *Papanikolaou et al.*, 2005] and is confirmed by other ^{36}Cl data [*Schlagenhauf*, 2009]. Measured vertical offsets across the scarps are between 3 m and 24 m, constrained by scarp profiles at 102 sites with the slope angle measured every meter; this indicates typical rates of vertical motion (throw-rates) between 0.2 and 1.6 mm/yr across individual faults [*Roberts and Michetti*, 2004; *Papanikolaou et al.*, 2005] (see fieldwork data presented in Table S2).

[10] Although overall the faults are dip-slip and dip to the SW, the kinematics are complicated by the fact that slip-directions converge towards the hanging walls (see Figures 1 and 2). Such variations are now well-documented for normal fault systems both from field measurements and from modeling fault growth [*Michetti et al.*, 2000; *Roberts and Michetti*, 2004; *Roberts*, 2007; *Maniatis and Hampel*, 2008]. In detail, outcrop observations show that fault planes are covered in millimeter-scale striations (frictional wear striae) and meter-scale corrugations that indicate the azimuth and plunge of the slip direction. Such features record motions in earthquakes, evidenced by formation of striations on fault planes at the bases of scarps that are freshly-exposed by slip in historical earthquakes [e.g., *Jackson et al.*, 1982; *Roberts*, 1996]. A large database at 155 sites constrains the slip directions at numerous sites along the active normal faults within the study area (see Figure 1) [*Morewood and Roberts*, 2000; *Roberts and Michetti*, 2004; *Papanikolaou et al.*, 2005; *Roberts*, 2007] (see new fieldwork data presented in Table S2).

[11] These combined throw-rate and slip-vector data sets were augmented by observations for the Laga fault made by *Galadini and Galli* [2000], the Ocre Fault by *Salvi et al.* [2003] and the throw-rate in the center of the Fucino basin fault estimated using InSAR [*Pizzi and Pugliese*, 2004]. (See Text S1.)[1]

[12] *Roberts* [2006] used measurements of slip direction and throw rates over 15 ± 3 ka to calculate velocities in the approximate regional strain direction, 225°, (Table 1), but did not calculate strain tensors, prompting this study.

[13] GPS measurements have been used to calculate strain-rates across the Apennines on timescales of 5–126 years [*D'Agostino et al.*, 2001a; *Hunstad et al.*, 2003; *Anzidei et al.*, 2005; *Serpelloni et al.*, 2005] (see Table 1 for a summary). Analysis of continuous and survey-mode GPS observations collected between 1991 and 2002 combining local, regional and global networks into a common reference frame over a comparable area to this study (sub-net 14, approximately 180 km × 80 km) found the principal horizontal strain-rate to be $3.1 \pm 0.8 \times 10^{-8}$ yr^{-1} and $3.7 \pm 2.8 \times 10^{-9}$ yr^{-1} parallel and

[1] Auxiliary materials are available in the HTML. doi:10.1029/2009JB006462.

perpendicular to 066° ± 7° respectively, implying an extension rate of 2.5 mm yr^{-1} [*Serpelloni et al.*, 2005]. During the time span 1999–2003, GPS measurements were used to calculate the principal strain-rates in an area ~180 km × 130 km from the Tyrrhenian to the Adriatic Sea (a greater across strike area than our study area; this was calculated as ranging from $12 \times 10^{-9} \pm 11$ yr^{-1} to $16 \times 10^{-9} \pm 11$ yr^{-1} and from $-14 \times 10^{-9} \pm 11$ yr^{-1} to $-3 \times 10^{-9} \pm 11$ yr^{-1} normal to and along the mountain chain respectively (depending which network data set is used) [*Anzidei et al.*, 2005]. Through analysis of the deformation of a sub-network of the National GPS Geodetic network IGM95 in the interval 1994–1999, the strain-rate in an area of approximately 35 km × 40 km (similar to the area covered by squares E, F, K and L in Figure 4) was calculated to be $1.8 \pm 0.3 \times 10^{-7}$ yr^{-1} , consistent with an extension rate of 6 ± 2 mm yr^{-1} [*D'Agostino et al.*, 2001a]. Shear strain-rates within the Lazio-Abruzzo region of the central Apennines averaged over 126 years calculated using a GPS reoccupation of the triangulation network were found to range up to 1.1×10^{-7} yr^{-1} in areas $\approx 10^3$ km^2, which suggests an extension rate between 2.5 mm yr^{-1} and 5 mm yr^{-1} assuming that the observed shear strains reflect only NE–SW extension and that the belt of deformation is 30–50 km wide [*Hunstad et al.*, 2003].

[14] Italy also has a long historical record that documents the magnitudes and locations of historical earthquakes. The CFTI catalogue can be searched to find large magnitude earthquakes that occurred in the central Apennines [*Guidoboni et al.*, 2007]. Italy has been urbanized since the Middle Ages and modern towns have buildings with comparable vulnerability to large earthquakes as those of the past [*Slejko et al.*, 1998], hence the CFTI catalogue is thought to be complete for earthquakes above magnitude 4.5 since 1000 A. D. [*Vorobieva and Panza*, 2004]. *Selvaggi* [1998] used these data to perform a summation of moment tensors of earthquakes with a moment magnitude greater than 6.0 over a time period of 700 years to calculate strain-rates across the whole of Italy. The inferred extension rate for the central Apennines from historical seismicity is 1.6 mm yr^{-1} [*Selvaggi*, 1998]. This does not include the 6th April 2009 Ms 6.3 L'Aquila earthquake, so we have augmented the data from *Selvaggi* [1998] with data from the L'Aquila earthquake.

[15] Below we compare strain-rates from moment summations, geodetic measurements and 15 ± 3 kyrs of fault slip across fault scarps by presenting a method that allows us to calculate strain-rates from fault slip in the same areas as those in Table 1.

3. Method

3.1. Calculation of Strain-Rates

[16] It is common for strains to be calculated from seismic moment release or geodetic data using techniques adapted from *Kostrov* [1974]. However, in this study we wished to find the strain-rates in the region from fault slip-rate data measured from outcropping striated fault planes, and compare our results with those from seismic moment release or geodetic data. We decided to adapt the techniques of *Kostrov* [1974] to (1) express the strain-rate tensor in terms of components that can be measured at outcrop where slip-rate data are collected, and (2) facilitate comparison with seismic moment release and geodetic studies. First, we explain how we adapted the techniques of *Kostrov* [1974] following the lead of other workers [*Holt and Haines*, 1995; *England and Molnar*, 1997], and second we explain how our field measurements were made and how they were implemented in the strain-rate calculations.

[17] *Kostrov* [1974] demonstrated that if all the strain in a volume is seismic and the dimensions of the faults are small relative to the region the average strain tensor, $\bar{\varepsilon}_{ij}$, within the volume can be obtained by summing the moment tensors of all the earthquakes occurring along faults within it:

$$\bar{\varepsilon}_{ij} = \frac{1}{2\mu V} \sum_{k=1}^{K} M_{ij}^{k} \tag{1}$$

where $\bar{\varepsilon}_{ij}$ represents the ith component of strain acting on the plane normal to the jth axis, M_{ij}^{k} is the ijth component of the moment tensor of the kth earthquake occurring within a volume V, and μ is the shear modulus. K is the total number of earthquakes in the volume V. k will consistently be used as a label, not as a power index, in the following equations.

[18] The moment tensor of an earthquake is by definition:

$$M_{ij} = M_0 \left(\hat{u}_i \hat{n}_j + \hat{u}_j \hat{n}_i \right) \tag{2}$$

$i, j = 1, 2, 3$ where $\hat{u}$ is a unit vector in the direction of slip, $\hat{n}$ is a unit vector normal to the fault plane (see Figure 2), $\hat{u}_i$ is the component of $\hat{u}$ in the direction of the ith axis, and M_0 is the scalar seismic moment, which is proportional to the average slip on the fault (s) in an earthquake and the area of the fault plane ruptured (A):

$$M_0 = \mu A s \tag{3}$$

Combining equations (1) and (2), substituting in the expression for scalar seismic moment and dividing by the time period of observation, gives:

$$\dot{\bar{\varepsilon}}_{ij} = \frac{1}{2\mu V t} \sum_{k=1}^{K} \mu A^{k} \bar{s}^{k} \left(\hat{u}_i^{k} \hat{n}_j^{k} + \hat{u}_j^{k} \hat{n}_i^{k} \right) \tag{4}$$

where $\dot{\bar{\varepsilon}}_{ij}$ is the average strain-rate tensor, $\bar{s}$ refers to the total slip from all earthquakes occurring on a given fault in time t. k now refers to each fault, rather than each earthquake on a fault and K is the number of faults in the volume V. Implicit to this method is the assumption that all the faults in the region are known. The 15 ± 3kyr strain-rates measured in this paper only include faults exposed at the surface, so we do not record strains from earthquakes below the threshold for surface slip, which is M 5.5 in the Apennines (see *Michetti et al.* [2000] for a review). By only including faults exposed at the surface we are assuming that the contribution to the strain-rate from smaller faults is not significant [*Scholz and Cowie*, 1990]. Note a similar threshold is used for the summation of moment tensors [*Selvaggi*, 1998].

[19] *Molnar* [1983] showed that equation (1) holds for a region whose dimensions are smaller than the length of the faults; the strain-rate is calculated by summing the moment rate released on the length of each fault segment within the volume. *England and Molnar* [1997] used the result of *Molnar* [1983] to express equation (4) in terms of parameters that can be measured in the field, without *a priori* knowledge of the thickness of the seismogenic layer or the shear modulus in the region.

[20] Replacing A^k with $\frac{wL^k}{\sin\vartheta^k}$, where w is the thickness of the faulted layer, ϑ^k is the dip of the fault, L^k is the length of the part of the fault contained within the volume V, and replacing V with aw, where a is the surface area of the region concerned, and simplifying the expression, removes μ and w from the expression [*England and Molnar*, 1997]:

$$\dot{\bar{\varepsilon}}_{ij} = \frac{1}{2at}\sum_{k=1}^{K}\frac{L^k\bar{s}^k}{\sin\vartheta^k}\left(\hat{u}_i^k\hat{n}_j^k + \hat{u}_j^k\hat{n}_i^k\right) \tag{5}$$

Measurements which are possible to take in the field include the strike (Φ), dip (ϑ), slip direction (ϕ), plunge (p), throw (T) and length of the fault (L). A flat earth approximation is used for the region considered as it only spans a few degrees latitude and longitude; the curvature of the earth becomes important when the region considered covers more than 10°–15° [*Haines and Holt*, 1993].

[21] The slip can be calculated from the measurement of throw using:

$$\bar{s} = \frac{T}{\sin p} \tag{6}$$

If strike is measured clockwise from north, then the 1, 2 and 3 axes correspond to east, north and vertically upwards respectively. The components of the slip vector, $\hat{u}$ (of unit magnitude), can be expressed as follows:

$$\hat{u}_1 = \sin\phi\cos p \tag{7}$$

$$\hat{u}_2 = \cos\phi\cos p \tag{8}$$

$$\hat{u}_3 = -\sin p \tag{9}$$

The components of the pole to the fault plane (of unit magnitude), $\hat{n}$, can be expressed as follows:

$$\hat{n}_1 = \cos\Phi\sin\vartheta \tag{10}$$

$$\hat{n}_2 = -\sin\Phi\sin\vartheta \tag{11}$$

$$\hat{n}_3 = \cos\vartheta \tag{12}$$

Thus the horizontal components of the strain-rate tensor can be written as follows:

$$\dot{\bar{\varepsilon}}_{11} = \frac{1}{at}\sum_{k=1}^{K}L^kT^k\cot p^k\sin\phi^k\cos\Phi^k \tag{13}$$

$$\dot{\bar{\varepsilon}}_{22} = -\frac{1}{at}\sum_{k=1}^{K}L^kT^k\cot p^k\cos\phi^k\sin\Phi^k \tag{14}$$

$$\dot{\bar{\varepsilon}}_{12} = \dot{\bar{\varepsilon}}_{21} = \frac{1}{2at}\sum_{k=1}^{K}L^kT^k\cot p^k\cos\left(\phi^k+\Phi^k\right) \tag{15}$$

It is useful to express the strain-rate tensors in terms of the principal strain-rates on principal axes as this makes their physical interpretation more significant. The horizontal principal axes correspond to maximum and minimum strain-rate directions within the horizontal plane and the principal strain-rates are the values in these directions.

[22] θ is the angle measured counter-clockwise between the "1" coordinate axes of the measured strain-rate tensor and the principal horizontal axis direction, it is found using:

$$\tan 2\theta = 2\frac{\dot{\bar{\varepsilon}}_{12}}{\dot{\bar{\varepsilon}}_{11}-\dot{\bar{\varepsilon}}_{22}} \tag{16}$$

ψ is the principal angle measured clockwise from north (i.e. $\psi = 90 - \theta$).

[23] The maximum horizontal average strain-rate ($\dot{\bar{\varepsilon}}'_{1'1'}$) and minimum horizontal average strain-rate ($\dot{\bar{\varepsilon}}'_{2'2'}$) are found using:

$$\dot{\bar{\varepsilon}}'_{1'1'} = \left(\frac{\dot{\bar{\varepsilon}}_{11}+\dot{\bar{\varepsilon}}_{22}}{2}\right) + \left(\frac{\dot{\bar{\varepsilon}}_{11}-\dot{\bar{\varepsilon}}_{22}}{2}\right)\cos 2\theta + \dot{\bar{\varepsilon}}_{12}\sin 2\theta \tag{17}$$

$$\dot{\bar{\varepsilon}}'_{2'2'} = \left(\frac{\dot{\bar{\varepsilon}}_{11}+\dot{\bar{\varepsilon}}_{22}}{2}\right) - \left(\frac{\dot{\bar{\varepsilon}}_{11}-\dot{\bar{\varepsilon}}_{22}}{2}\right)\cos 2\theta - \dot{\bar{\varepsilon}}_{12}\sin 2\theta. \tag{18}$$

[24] Equations (16), (17) and (18) are derived by *Fung* [1977]. The 1′ and 2′ axes correspond to the maximum horizontal strain-rate direction and the direction orthogonal to it respectively. Expressing (16), (17) and (18) in terms of independent components that can be measured in the field gives:

$$\theta = \frac{1}{2}\arctan\left(\frac{\sum_{k=1}^{K}L^kT^k\cot p^k\cos\left(\phi^k+\Phi^k\right)}{\sum_{k=1}^{K}L^kT^k\cot p^k\sin\left(\phi^k+\Phi^k\right)}\right) \tag{19}$$

$$\dot{\bar{\varepsilon}}'_{1'1'} = \frac{1}{2at}\sum_{k=1}^{K}\left\{L^kT^k\cot p^k\left[\sin\left(\phi^k-\Phi^k\right) + \sin\left(\phi^k+\Phi^k+\arctan\left(\frac{\sum_{k=1}^{K}L^kT^k\cot p^k\cos\left(\phi^k+\Phi^k\right)}{\sum_{k=1}^{K}L^kT^k\cot p^k\sin\left(\phi^k+\Phi^k\right)}\right)\right)\right]\right\} \tag{20}$$

$$\dot{\bar{\varepsilon}}'_{2'2'} = \frac{1}{2at}\sum_{k=1}^{K}\left\{L^kT^k\cot p^k\left[\sin\left(\phi^k-\Phi^k\right) - \sin\left(\phi^k+\Phi^k+\arctan\left(\frac{\sum_{k=1}^{K}L^kT^k\cot p^k\cos\left(\phi^k+\Phi^k\right)}{\sum_{k=1}^{K}L^kT^k\cot p^k\sin\left(\phi^k+\Phi^k\right)}\right)\right)\right]\right\}. \tag{21}$$

[25] Equations (19), (20) and (21) are used to calculate the horizontal components of the average strain-rate tensor in the horizontal principal directions within volumes with square surface areas on a Universal Transverse Mercator (UTM) map projection within the Italian Apennines. The squares were arranged with their edges aligned along NW–SE and

NE–SW axes parallel and perpendicular to the orientations of the faults. For comparisons with strain-rates calculated from other input data (geodetic and seismic), the 5 km square areas were combined to match the areas defined by other authors. Where an exact match could not be made, care was taken to ensure that the same proportion of fault traces of each fault were included in the regions being compared. Matches of polygon vertices are within a few km of the actual locations (Figures 6 and 7).

[26] For the comparison with the geodetic data of *Hunstad et al.* [2003], the results are expressed in terms of the shear strains (note that equations (19) and (24) are equivalent):

$$\begin{aligned}\gamma_1 &= \frac{\delta u_1}{\delta x_1} - \frac{\delta u_2}{\delta x_2} \\ &= \dot{\bar{\varepsilon}}_{11} - \dot{\bar{\varepsilon}}_{22} \\ &= \frac{1}{at}\sum_{k=1}^{K}\left\{L^k T^k \cot p^k \sin\left(\phi^k + \Phi^k\right)\right\}\end{aligned} \tag{22}$$

$$\begin{aligned}\gamma_2 &= \frac{\delta u_1}{\delta x_2} + \frac{\delta u_2}{\delta x_1} \\ &= 2\dot{\bar{\varepsilon}}_{12} \\ &= \frac{1}{at}\sum_{k=1}^{K}\left\{L^k T^k \cot p^k \cos\left(\phi^k + \Phi^k\right)\right\}\end{aligned} \tag{23}$$

$$\begin{aligned}\theta &= \frac{1}{2}\arctan\left(\frac{\gamma_2}{\gamma_1}\right) \\ &= \frac{1}{2}\arctan\left(\frac{\sum_{k=1}^{K}\left\{L^k T^k \cot p^k \cos\left(\phi^k + \Phi^k\right)\right\}}{\sum_{k=1}^{K}\left\{L^k T^k \cot p^k \sin\left(\phi^k + \Phi^k\right)\right\}}\right).\end{aligned} \tag{24}$$

[27] The summed earthquake seismic moments over a period of 700 years for earthquakes larger than 1.2×10^{25} dyne.cm (1.2×10^{18} Nm, corresponding to a moment magnitude of c. 6.0) have been calculated [*Selvaggi*, 1998]. The strain bar lengths and angles were measured from the principal strain-rate map in the paper by *Selvaggi* [1998] and the strain from the L'Aquila 2009 earthquake was added to this data set.

[28] Faults were mapped in the field with a hand-held GPS onto 1:100000 topographic and geological maps and SRTM topographic data by identifying fault scarps (and new fieldwork, see Table S2) [*Roberts and Michetti*, 2004]; traces were improved by mapping within Google Earth that allows fault traces to be constrained to within a few meters [*Roberts*, 2008]. Geological mapping of the region has complete coverage with faults identified that have total throws as small as a few tens of meters [e.g., *Vezzani and Ghisetti*, 1998]; each of these faults has been checked for signs of Holocene slip. Additional information on the locations of faults that have produced Holocene offsets during large magnitude earthquakes is provided by paleoseismological trench site data [*Giraudi and Frezzotti*, 1995; *Michetti et al.*, 1996; *Pantosti et al.*, 1996; *Galadini et al.*, 1997; *Galadini and Galli*, 1999; *D'Addezio et al.*, 2001; *Moro et al.*, 2002; *Galadini and Galli*, 2003; *Salvi et al.*, 2003]. A surface fault map was produced showing how the faults appear at the surface (Figure 1). The connectivity of fault segments at depth and the lengths and positions of individual faults were assessed using slip directions, total throw since fault initiation (c. 3 Ma) and throws since 12–18 ka. Specifically, the lateral tips of faults are defined at places where 12–18 ka slip decreases to zero, the cumulative offset of Mesozoic strata decrease to zero, and where slip directions change across fault segment boundaries (see *Roberts and Michetti* [2004] for details). We smoothed the fault map at depth so that fault traces are straight within individual 5 km × 5 km grid squares in our calculations (Figure 8). This was done so that the length of the fault segment at depth was not biased by the detail of the surface mapping. Slip-rate and slip direction data are interpolated linearly between locations where data have been collected and where the faults cross grid lines. At the ends of the faults where commonly no fault plane is exposed at the surface, the 12–18 ka throw is assigned as zero. As the tips of the faults are generally poorly exposed, the slip vectors at the tips of the faults are assigned as almost strike-slip towards the center of the fault with a 20° dip-slip component, this corresponds to values measured at sites found closest to the tips of faults [*Morewood and Roberts*, 2000; *Roberts and Michetti*, 2004; *Roberts*, 2007]. In the case of faults which have measured slip directions which do not suggest a converging slip pattern (Tre-Monti Fault and Velino-Magnola Fault), the slip direction and plunge at the tips are assigned the values measured closest to the tips, which are in any case measured within 1.5 km of the tips.

3.2. Errors

[29] An error of ±5° was assigned to the slip direction and plunge of the slip-vector as this is the mean 99% confidence level defined statistically in stereographic projection software (available at www.geo.cornell.edu/geology/faculty/RWA/programs.html) [*Roberts and Michetti*, 2004; *Roberts*, 2007]. Likewise, the error estimated for the fault strike is ±5°. The age of the scarps has an error of ±20% (corresponding to the ±3 kyr uncertainty). The throw since 15 ± 3 ka has an uncertainty of ±20% because this is the natural variability in the throw across scarps that we have measured in the field using total stations and lidar laser scanners within a few tens of meters along strike of a given scarp profile [e.g., *Roberts and Michetti*, 2004] and due to fitting lines to slopes on scarp profiles. Detailed geomorphic mapping has confirmed there is not a regional lateral change in erosion rate. Scarps with Late Pleistocene-Holocene maximum offsets of 2.7 ± 0.5 m (Ventrino Fault) and 3.0 ± 0.6 m (Pescocostanzo Fault) have been identified (see Table S2) and post 15 ± 3 ka throws as small as 0.4 ± 0.1 m [*Morewood and Roberts*, 2000] have been measured; hence, in these locations slope erosion and sedimentation processes must operate at rates much lower than 0.3 ± 0.1 mm/yr as they are too slow to obscure the scarps. Therefore, following *Roberts* [2006], we assume that we and other workers will have been able to identify all scarps with post 15 ± 3 ka throws greater than a few meters as the scarps commonly occur high on mountain slopes and can be seen from several kilometers away. A scarp with a post 15 ± 3 ka throw less than a few meters would increase the regional strain-rate by approximately 1%, which is significantly less than the stated errors of the regional strain-rate magnitude. Our conclusion that we have identified all scarps with post 15 ± 3 ka throws greater than a few meters is supported by the observation that our scarp map compares almost exactly with that of

other workers [e.g., *Piccardi et al.*, 1999; *Galadini and Galli*, 2000], where faults are assigned as active; this indicates that a consensus exists on active fault locations and numbers. Such faults have produced hundreds of meters of cumulative throw over the 2–3 Myr timescale that they have been active [see *Roberts and Michetti*, 2004], despite their low throw rates. This explains why our scarp map compares so well with those of other workers; faults with total throws as large as a few hundred meters are probably completely recognized within the area considered due to excellent exposure and extremely detailed geological mapping conducted over many decades (see *Vezzani and Ghisetti* [1998] for a compilation of this mapping). Thus, we doubt that we and other workers have significantly underestimated the geological strain-rates due to non-identification of active faults. However, note that the Database of Individual Seismogenic Sources (DISS) [*Basili et al.*, 2008] does not include some of the active faults described herein and in previous studies [*Roberts and Michetti*, 2004; *Papanikolaou et al.*, 2005]. The error in the total length of each fault we consider to be active is +10% as the fault tips are difficult to trace at the surface. The error propagating from the uncertainty in the location of fault tips is minimal as the post 15 ± 3 ka throw is very small in these locations (<1–2 meters) and hence the contribution to the 15 ± 3 kyr strain-rate is very small. On the 5 km scale strain-rate map (Figure 3), where no faults occur within given grid squares, the strain is calculated as zero. Thus, the uncertainty in location of the fault tips may cause errors where the fault extends into an area where no fault is shown. The error in the strain-rate derived from the error in the length is only relevant for grid squares at fault tips, where the strain is small in any case. Therefore, an error of 5% of the total fault length is assigned in grid boxes which contain a fault tip. Grid boxes not containing a fault tip are assigned a zero error for fault length.

4. Results

[30] Our method allows us to report strain-rates in any 5 km × 5 km grid square or any combination of these grid squares. This allows us to compare strain-rates from 15 ± 3 kyr of slip with those from shorter time periods within polygons that are comparable in size, shape and location to those imposed by geodetic station locations or moment summation calculations.

[31] Within the entire area containing the mapped active normal faults of 1.28×10^4 km^2 (80 km × 160 km, see grid in Figures 3 and 4) the average horizontal strain-rate over the last 15 kyrs is $1.18^{+0.12}_{-0.04} \times 10^{-8}$ yr^{-1} along the horizontal axis parallel to 043°–223° ± 1° and $-1.83^{+3.80}_{-4.43} \times 10^{-10}$ yr^{-1} perpendicular to it (for previous estimates of strain-rate see Table 1). The strain-rate along the principal axis is approximately 2.6 × less than $3.1 \pm 0.8 \times 10^{-8}$ yr^{-1}, calculated by GPS over a similar area [*Serpelloni et al.*, 2005]. The strain-rate perpendicular to the principal axis is an order of magnitude less than $3.7 \pm 2.8 \times 10^{-9}$ yr^{-1}, calculated using GPS [*Serpelloni et al.*, 2005].

[32] The 15 ± 3 kyr extension rate across the central Apennines, implied by strain-rates within the 80 km × 160 km area of the grid shown in Figures 3 and 4 is 1.0 ± 0.1 mm yr^{-1}, although note that this contains low strain-rate areas at the NW and SE ends of the grid, and presumably undeforming areas along the NE and SW edges of the grid. This average value is less than 2.5–5.0 mm yr^{-1} calculated using geodesy [*Hunstad et al.*, 2003] and 1.6 ± 0.5 mm yr^{-1} calculated using summation of moment tensors [*Selvaggi*, 1998]. However, extension rates calculated from the strain-rates along 5 km wide transects perpendicular to the axis of the mountain chain multiplied by the length of the transects (80 km), vary from 0.02 ± 0.01 mm yr^{-1} up to $3.1^{+0.7}_{-0.4}$ mm yr^{-1} (Figure 5). The maximum value for such transects is within the range implied by 1-dimensional addition of horizontal slip rates averaged over the same time period (4.3 ± 1.7 mm yr^{-1}) [*Roberts*, 2006], geodesy [*Hunstad et al.*, 2003], and summation of moment tensors [*Selvaggi*, 1998]. Note also that an early attempt to calculate extension rates using GPS over a time period of 5 years in an area 35 km × 70 km (similar to area covered by squares E, F, K and L in Figure 4) gave a value of 6 ± 2 mm yr^{-1} [*D'Agostino et al.*, 2001a]; over the same area the extension rate calculated from Late Pleistocene-Holocene fault scarps is 1.7 ± 0.1 mm yr^{-1}.

[33] At a smaller scale, within individual 5 km × 5 km grid squares, the horizontal average principal strain-rates vary from zero up to $2.34 \pm 0.54 \times 10^{-7}$ yr^{-1} (Table 2). Both the magnitude and direction of strain-rates vary along the strike of individual faults. The strain-rate at this length-scale is highest in grid squares containing the centers of the Fucino, Liri and Sulmona faults.

[34] Within individual 20 km × 20 km grid square areas, the horizontal average principal strain-rates vary from zero up to $4.43^{+3.21}_{-0.64} \times 10^{-8}$ yr^{-1} (Table 3). The grid box containing the Fucino basin has the highest strain-rate at this scale, with strain-rates decreasing systematically both along strike and across strike from this location.

[35] Strain-rates in 5 km × 80 km transects orientated perpendicular to the mountain chain axis are highest in the center of the study region and decrease to the NW and SE (Figure 5). At the SE end of the study area the strain-rates in the transects are calculated across a single fault and thus the change in throw along the strike of the fault is reflected in the change in strain-rates along the axis of the Apennines. NW of the Fucino Plain, despite the transects containing the middle of some faults and tips of others the strain-rates are fairly uniform along the axis of the mountain chain, thus the signature from individual faults is less dominant.

[36] Comparison of strain-rates calculated over 15 ± 3 kyrs with those over 10^2 yrs from seismic summations and GPS re-occupation of triangulation sites shows that the strain-rate is not the same over different time periods (Tables 4 and 5). Figures 6 and 7 show that in the NE, the 10^2 yr strain-rate is higher than that averaged over 15 ± 3 kyrs (polygon 30 Figure 6 and polygons 7 and 8 Figure 7). In the SE of the study area, the strain-rates over the different time periods are comparable (polygons 33 and 36 Figure 6). In the SW of the study area the 15 ± 3 kyr strain-rates are higher than the 10^2 yr strain-rates calculated from moment tensor summation (polygons 32, 35 and 38 Figure 6) because no earthquakes are assigned to these areas [*Selvaggi*, 1998]; the strain-rates calculated from geodesy in the SW (polygons 2 and 3 Figure 6) have an absolute value less than their error.

5. Discussion

[37] Our results show for the first time how strain-rates vary on a length scale less than that of individual faults

Table 2. Average Horizontal Principal Strain-Rates Calculated in 5 km × 5 km Areas Using Measurements From Striated Faults Offsetting Late Pleistocene-Holocene Features[a]

X UTM Mid Point of Grid Square	Y UTM Mid Point of Grid Square	Principal Strain-Rate ($\dot{\bar{\varepsilon}}'_{1'1'}$/yr^{-1})	Strain-Rate Normal to Principal Strain-Rate Direction ($\dot{\bar{\varepsilon}}'_{2'2'}$/yr^{-1})	Principal Angle Azimuth (ψ/deg)
415668	4588909	8.77 ± 4.16E-09	−5.60 ± 3.93E-09	047 ± 4
412132	4592444	5.91 ± 1.65E-08	*−0.07 ± 1.32E-08*	053 ± 3
408597	4595980	4.66 ± 1.46E-08	*−0.19 ± 1.17E-08*	037 ± 3
405061	4599515	2.34 ± 0.66E-08	−7.73 ± 5.50E-09	026 ± 3
401525	4603051	4.79 ± 2.05E-09	−2.92 ± 1.91E-09	018 ± 4
383848	4627800	1.95 ± 1.48E-08	*−0.72 ± 1.44E-08*	073 ± 4
380312	4631335	9.27 ± 3.34E-08	*−0.48 ± 2.77E-08*	059 ± 4
376777	4634871	2.34 ± 0.54E-07	*−0.12 ± 4.36E-08*	039 ± 3
373241	4638406	1.07 ± 0.31E-07	*−0.46 ± 2.53E-08*	048 ± 3
369706	4641942	6.70 ± 2.81E-08	*−0.22 ± 2.48E-08*	044 ± 4
366170	4645477	8.54 ± 3.24E-08	*−0.00 ± 2.82E-08*	034 ± 3
362635	4649013	7.86 ± 2.05E-08	*−1.09 ± 1.69E-08*	025 ± 3
359099	4652548	7.80 ± 2.32E-08	*−2.17* ± 1.92E-08	001 ± 3
355563	4656084	*1.55 ± 2.62E-08*	*−1.04 ± 2.60E-08*	016 ± 17
352028	4659619	3.80 ± 1.85E-09	−1.93 ± 1.73E-09	078 ± 4
348492	4663155	2.83 ± 0.57E-08	−7.03 ± 4.76E-09	067 ± 3
344957	4666691	3.39 ± 0.92E-08	*−0.07 ± 7.75E-09*	052 ± 3
341421	4670226	1.37 ± 0.54E-08	*−1.41 ± 4.67E-09*	028 ± 4
337886	4673762	*2.59 ± 2.86E-10*	*−1.21 ± 2.82E-09*	023 ± 4
369706	4649013	*1.32 ± 3.26E-10*	*0.00 ± 3.25E-10*	054 ± 8
366170	4652548	9.36 ± 3.43E-09	*−0.06 ± 2.88E-09*	057 ± 4
362635	4656084	2.62 ± 0.93E-08	*−0.41 ± 7.67E-09*	046 ± 4
359099	4659619	4.78 ± 1.65E-08	*−0.12 ± 1.35E-08*	046 ± 4
355563	4663155	6.75 ± 2.07E-08	*−0.16 ± 1.69E-08*	044 ± 3
352028	4666691	7.42 ± 2.63E-08	*−0.01 ± 2.17E-08*	048 ± 4
348492	4670226	7.51 ± 2.77E-08	*−0.01 ± 2.33E-08*	043 ± 4
344957	4673762	*3.34 ± 7.01E-08*	*−0.03 ± 6.98E-08*	041 ± 24
390919	4634871	3.93 ± 2.28E-08	*−0.80 ± 2.18E-08*	071 ± 4
387383	4638406	1.11 ± 0.37E-07	*−0.82 ± 3.02E-08*	056 ± 4
383848	4641942	1.38 ± 0.32E-07	*−0.69 ± 2.56E-08*	068 ± 3
380312	4645477	5.62 ± 1.17E-08	*−2.39 ± 9.36E-09*	044 ± 2
376777	4649013	2.54 ± 0.86E-08	*−4.45 ± 6.99E-08*	027 ± 4
373241	4652548	*5.85 ± 7.40E-10*	*−2.66 ± 7.33E-09*	027 ± 4
369706	4656084	5.45 ± 0.98E-10	*−0.88 ± 5.11E-12*	161 ± 5
355563	4670226	*0.22 ± 1.33E-10*	*−0.10 ± 1.33E-10*	063 ± 4
352028	4673762	2.54 ± 0.51E-08	*−1.16 ± 4.17E-09*	058 ± 2
348492	4677297	1.56 ± 0.53E-08	*−0.01 ± 4.24E-09*	058 ± 4
344957	4680833	1.22 ± 0.25E-07	*−1.64 ± 2.07E*-08	032 ± 2
341421	4684368	1.10 ± 0.28E-07	*−0.01 ± 2.30E-08*	046 ± 3
337886	4687904	8.12 ± 3.52E-08	*−1.34 ± 3.14E-08*	034 ± 4
330815	4694975	5.81 ± 2.33E-09	−2.98 ± 2.16E-09	086 ± 3
327279	4698510	6.58 ± 2.76E-09	*−0.65 ± 2.43E-09*	086 ± 4
408597	4624264	1.23 ± 0.34E-07	−3.80 ± 3.03E-08	038 ± 3
405061	4627800	1.44 ± 0.41E-07	*−0.30 ± 3.34E-08*	044 ± 3
401525	4631335	7.27 ± 1.81E-08	*−0.62 ± 1.47E-08*	035 ± 3
397990	4634871	1.41 ± 0.35E-08	*−1.63 ± 3.03E-09*	023 ± 3
394454	4638406	1.17 ± 0.32E-08	*−0.41 ± 2.35E-09*	036 ± 4
373241	4659619	1.31 ± 0.07E-08	*−0.18 ± 6.71E-11*	159 ± 1
369706	4663155	5.03 ± 1.04E-08	*−0.60 ± 8.78E-09*	019 ± 2
366170	4666691	7.99 ± 1.89E-08	*−0.61 ± 1.52E-08*	028 ± 3
362635	4670226	7.53 ± 1.93E-09	−1.79 ± 1.60E-09	018 ± 3
359099	4673762	2.79 ± 1.88E-10	*−0.69 ± 1.80E-10*	017 ± 4
352028	4680833	7.96 ± 2.67E-08	*−0.01 ± 2.15E-08*	057 ± 4
348492	4684368	4.51 ± 1.53E-08	*−0.65 ± 1.24E-08*	033 ± 4
330815	4702046	5.77 ± 2.54E-09	*−0.16 ± 2.38E-09*	078 ± 3
327279	4705581	4.76 ± 3.31E-09	*−0.46 ± 3.17E-09*	053 ± 4
323744	4709117	2.40 ± 0.69E-08	*−0.42 ± 5.63E-09*	027 ± 4
415668	4624264	1.73 ± 0.63E-08	−1.62 ± 0.62E-08	050 ± 4
412132	4627800	2.06 ± 0.52E-08	−1.15 ± 0.46E-08	045 ± 3
397990	4641942	2.14 ± 0.49E-09	*−2.06 ± 2.70E-10*	097 ± 10
394454	4645477	$4.31^{+4.30}_{-3.62}$E-08	$-0.26^{+3.60}_{-3.90}$*E-08*	061 ± 11
390919	4649013	$1.23^{+1.10}_{-0.23}$E-07	$-0.22^{+1.98}_{-3.36}$*E-08*	044 ± 2
387383	4652548	$1.22^{+2.04}_{-0.28}$E-07	$0.02^{+5.17}_{-2.29}$*E-08*	044 ± 3
383848	4656084	$1.22^{+1.85}_{-0.43}$E-07	$-0.35^{+3.54}_{-6.90}$*E-08*	043 ± 4
380312	4659619	$1.26^{+1.18}_{-0.45}$E-07	$-1.57^{+3.78}_{-6.04}$*E-08*	045 ± 4
376777	4663155	$1.59^{+0.42}_{-0.28}$E-07	$-2.48^{+2.34}_{-2.78}$E-08	041 ± 2
373241	4666691	3.72 ± 0.74E-08	*−2.21 ± 5.87E-09*	038 ± 3
355563	4684368	2.57 ± 1.41E-09	*−1.16 ± 1.40E-09*	092 ± 4

Table 2. (continued)

X UTM Mid Point of Grid Square	Y UTM Mid Point of Grid Square	Principal Strain-Rate ($\dot{\bar{\varepsilon}}'_{1'1'}$/yr^{-1})	Strain-Rate Normal to Principal Strain-Rate Direction ($\dot{\bar{\varepsilon}}'_{2'2'}$/yr^{-1})	Principal Angle Azimuth (ψ/deg)
352028	4687904	2.28 ± 0.77E-08	*−6.55 ± 6.38E-09*	076 ± 4
348492	4691439	4.34 ± 1.46E-08	*−0.15 ± 1.18E-08*	058 ± 4
344957	4694975	4.92 ± 1.26E-08	*0.00 ± 1.01E-08*	034 ± 3
341421	4698510	1.97 ± 0.68E-08	*−5.19 ± 5.61E-09*	032 ± 4
337886	4702046	1.10 ± 0.83E-09	*−6.14 ± 8.11E-10*	031 ± 4
327279	4712652	1.67 ± 0.66E-09	*−5.54 ± 5.84E-10*	037 ± 4
422739	4624264	*0.05 ± 2.40E-11*	*−0.02 ± 2.40E-11*	069 ± 4
419203	4627800	3.04 ± 1.13E-10	−3.91 ± 1.23E-10	054 ± 4
397990	4649013	1.58 ± 0.56E-08	*−0.11 ± 4.62E-09*	073 ± 4
394454	4652548	2.93 ± 1.58E-09	*−0.03 ± 1.53E-09*	065 ± 6
390919	4656084	1.43 ± 0.25E-08	*−0.08 ± 1.97E-09*	054 ± 3
387383	4659619	5.05 ± 1.83E-09	*−0.73 ± 1.54E-09*	054 ± 4
376777	4670226	9.05 ± 2.28E-08	*−1.51 ± 1.84E-08*	043 ± 2
373241	4673762	*3.22 ± 4.79E-08*	*0.19 ± 4.47E-08*	023 ± 46
369706	4677297	2.76 ± 0.57E-08	*−0.71 ± 4.97E-09*	030 ± 2
366170	4680833	1.77 ± 0.43E-08	*0.00 ± 3.48E-09*	035 ± 3
362635	4684368	1.09 ± 0.52E-09	*−2.87 ± 4.79E-09*	010 ± 4
334350	4712652	0.48 ± 5.29*E*-09	*−1.57 ± 0.62E-08*	114 ± 4
330815	4716188	1.27 ± 0.52E-08	*−2.39 ± 4.66E-09*	050 ± 3
422739	4631335	5.56 ± 1.97E-08	*−0.70 ± 1.85E-08*	060 ± 4
419203	4634871	3.83 ± 1.33E-08	*−0.97 ± 1.10E-08*	027 ± 4
415668	4638406	1.81 ± 0.94E-09	*−6.88 ± 8.77E-10*	002 ± 4
373241	4680833	2.79 ± 0.95E-09	*−2.75 ± 7.72E-10*	074 ± 4
369706	4684368	6.37 ± 1.59E-09	*−0.19 ± 1.28E-09*	044 ± 3
362635	4691439	1.57 ± 0.53E-09	*−0.35 ± 4.30E-09*	036 ± 4
359099	4694975	1.56 ± 0.71E-08	*−0.23 ± 6.56E-09*	015 ± 4
422739	4638406	2.15 ± 0.42E-08	*−0.49 ± 3.55E-09*	053 ± 2
419203	4641942	1.78 ± 0.49E-08	*−0.92 ± 4.08E-09*	042 ± 3
387383	4673762	3.86 ± 0.85E-09	−8.37 ± 3.90E-10	178 ± 4
373241	4687904	2.18 ± 0.74E-09	*−1.86 ± 6.37E-10*	035 ± 3
369706	4691439	1.33 ± 0.48E-09	*−1.40 ± 3.99E-10*	070 ± 4
366170	4694975	7.74 ± 2.20E-08	*−0.26 ± 1.80E-08*	041 ± 3
362635	4698510	4.62 ± 1.18E-08	*−0.15 ± 9.63E-09*	036 ± 3
359099	4702046	8.70 ± 1.75E-08	*−0.03 ± 1.41E-08*	047 ± 2
355563	4705581	1.54 ± 0.67E-08	*−4.03 ± 6.04E-09*	012 ± 3
426274	4641942	2.91 ± 2.01E-09	*−0.28 ± 1.93E-09*	063 ± 4
422739	4645477	1.59 ± 0.53E-08	*−1.77 ± 4.30E-09*	059 ± 4
397990	4670226	4.19 ± 2.45E-09	*−1.41 ± 2.32E-09*	071 ± 4
394454	4673762	4.90 ± 0.76E-08	*−0.48 ± 6.06E-09*	046 ± 2
390919	4677297	3.33 ± 1.10E-09	*−1.53 ± 9.02E-10*	010 ± 3
387383	4680833	2.89 ± 0.97E-08	*−2.03 ± 7.76E-09*	052 ± 4
383848	4684368	1.28 ± 0.35E-07	*−0.49 ± 2.83E-08*	051 ± 3
380312	4687904	9.83 ± 2.14E-08	*−0.08 ± 1.72E-08*	050 ± 2
376777	4691439	5.48 ± 1.78E-08	*0.00 ± 1.42E-08*	042 ± 3
373241	4694975	3.77 ± 1.25E-08	*−0.03 ± 9.99E-09*	029 ± 4
369706	4698510	2.84 ± 0.88E-08	*−0.06 ± 7.86E-09*	015 ± 3
366170	4702046	9.88 ± 2.05E-09	−6.40 ± 5.60E-10	161 ± 4
362635	4705581	1.04 ± 0.39E-08	*−0.95 ± 3.30E-09*	076 ± 4
359099	4709117	2.78 ± 0.81E-08	*−0.03 ± 6.57E-09*	048 ± 3
355563	4712652	1.08 ± 0.37E-08	*−1.63 ± 3.02E-09*	049 ± 4
426274	4649013	2.46 ± 0.83E-08	*−3.67 ± 6.72E-09*	057 ± 4
422739	4652548	6.81 ± 2.32E-08	−2.03 ± 1.92E-08	057 ± 4
419203	4656084	1.36 ± 0.82E-08	*−5.85 ± 7.81E-09*	041 ± 4
415668	4659619	1.40 ± 0.47E-07	*−0.46 ± 3.73E-08*	050 ± 4
412132	4663155	2.16 ± 0.56E-07	*−0.05 ± 4.44E-08*	046 ± 3
408597	4666691	1.46 ± 0.33E-07	*−0.83 ± 2.64E-08*	033 ± 3
405061	4670226	3.62 ± 1.17E-08	−2.33 ± 1.04E-08	016 ± 3
401525	4673762	*2.34 ± 6.44E-10*	*−1.27 ± 6.43E-09*	017 ± 4
394454	4680833	*3.82 ± 3.91E-08*	*−0.38 ± 3.89E-08*	065 ± 9
390919	4684368	7.24 ± 2.42E-08	*−0.65 ± 1.95E-08*	054 ± 4
380312	4694975	6.37 ± 3.15E-09	*−0.94 ± 3.03E-10*	006 ± 3
376777	4698510	7.56 ± 2.58E-08	*−0.01 ± 2.10E-08*	021 ± 4
373241	4702046	6.76 ± 2.39E-08	*−0.01 ± 1.98E-08*	014 ± 4
359099	4716188	6.07 ± 4.19E-10	*−2.41 ± 4.04E-10*	038 ± 4
426274	4656084	1.89 ± 0.65E-08	−7.12 ± 5.43E-09	054 ± 4
422739	4659619	1.04 ± 0.26E-07	−3.63 ± 2.19E-08	047 ± 3
419203	4663155	1.30 ± 0.45E-08	−5.68 ± 3.79E-09	043 ± 4
387383	4694975	1.42 ± 0.77E-08	*−2.73 ± 6.35E-09*	038 ± 11
383848	4698510	9.46 ± 2.08E-08	*0.04 ± 1.67E-08*	023 ± 3
380312	4702046	2.20 ± 0.34E-08	−2.85 ± 1.02E-09	178 ± 3

Table 2. (continued)

X UTM Mid Point of Grid Square	Y UTM Mid Point of Grid Square	Principal Strain-Rate ($\dot{\varepsilon}'_{1'1'}$/yr^{-1})	Strain-Rate Normal to Principal Strain-Rate Direction ($\dot{\varepsilon}'_{2'2'}$/yr^{-1})	Principal Angle Azimuth (ψ/deg)
376777	4705581	4.07 ± 0.93E-09	−1.15 ± 5.01E-09	167 ± 4
373241	4709117	*8.53 ± 8.78E-10*	*−3.30 ± 8.63E-10*	084 ± 4
369706	4712652	4.22 ± 1.54E-08	*−0.16 ± 1.28E-08*	067 ± 4
366170	4716188	7.89 ± 2.85E-08	*−0.42 ± 2.39E-08*	058 ± 3
362635	4719724	6.28 ± 1.65E-08	*−0.02 ± 1.37E-08*	047 ± 4
359099	4723259	5.76 ± 3.33E-09	*−1.42 ± 3.13E-09*	013 ± 4
422739	4666691	*0.84 ± 1.48E-09*	*−0.40 ± 1.47E-09*	041 ± 4
401525	4687904	1.36 ± 0.78E-08	*−2.27 ± 7.30E-09*	070 ± 4
397990	4691439	4.71 ± 1.44E-08	*−0.42 ± 1.22E-08*	068 ± 3
394454	4694975	3.06 ± 1.13E-08	*0.18 ± 9.53E-09*	032 ± 4
390919	4698510	1.23 ± 0.41E-07	*−0.12 ± 3.42E-08*	019 ± 3
387383	4702046	3.12 ± 0.86E-08	*−0.38 ± 7.27E-09*	012 ± 3
401525	4694975	2.57 ± 0.97E-08	*−3.36 ± 8.25E-09*	065 ± 4
397990	4698510	8.05 ± 2.50E-08	*−0.98 ± 2.11E-08*	034 ± 3

[a]The errors in the strain-rates within the Fucino Basin are asymmetrical (see Text S1). Strain-rates written in italics are those which have an absolute magnitude less than their error and thus the sign of the strain-rate is undetermined. The grid boxes are expressed in terms of the UTM coordinates of their mid points and all lie within UTM zone 33T.

(5 km and 20 km) and between 15 ± 3 kyr and 10^2 yr timescales in the central Apennines, Italy. The spatial variation in strain-rates shows that it is important to consider the exact same areas when comparing strain-rates measured using different time periods and techniques. We have compared areas that have edges within less than 3.5 km of each other when comparing strain-rates over different timescales (Figures 6 and 7). The above has not been achieved in other extending areas such as Greece and The Basin and Range [*Davies et al.*, 1997; *Friedrich et al.*, 2003; *Kreemer et al.*, 2004].

[38] The possibility that strain-rates might vary on the scale of individual faults was noted by *Hunstad et al.* [2003]. They concluded that "questions related to tectonics on the scale of 30 km or less will have to await data from denser GPS-to-GPS networks"; our results address this concern, but over a longer timescale than envisaged by *Hunstad et al.* [2003]. Our results also address the long-standing problem of how to compare strains measured within different-shaped polygons. Use of a regular grid that can be rotated to run parallel to the structures responsible for the deformation, and re-sized to approximate polygon shapes imposed

Table 3. Average Horizontal Principal Strain-Rates Calculated in 20 km × 20 km Areas Using Measurements From Striated Faults Offsetting Late Pleistocene-Holocene Features[a]

UTM X Mid Point of Grid Square	UTM Y Mid Point of Grid Square	Principal Strain-Rate ($\dot{\varepsilon}'_{1'1'}$/yr^{-1})	Strain Rate Normal to Principal Strain-Rate Direction ($\dot{\varepsilon}'_{2'2'}$/yr^{-1})	Principal Angle Azimuth (ψ/deg)
412132	4595980	8.30 ± 2.37E-09	*−0.67 ± 2.18E-09*	042 ± 3
397990	4610122	2.99 ± 1.28E-10	−1.83 ± 1.19E-10	018 ± 4
383848	4624264	6.93 ± 3.39E-09	*−0.67 ± 3.18E-09*	062 ± 4
369706	4638406	3.07 ± 0.47E-08	*−0.27 ± 3.89E-09*	041 ± 2
355563	4652548	1.80 ± 0.49E-08	*−0.54 ± 4.48E-09*	027 ± 7
341421	4666691	1.58 ± 0.56E-08	*−0.13 ± 5.42E-09*	048 ± 4
412132	4624264	1.90 ± 1.26E-08	*−0.42 ± 1.24E-08*	042 ± 6
397990	4638406	$1.80^{+0.48}_{-0.44}$ E-08	$-0.36^{+4.05}_{-4.17}$ *E-09*	053 ± 4
383848	4652548	$4.43^{+3.21}_{-0.64}$ E-08	$-0.64^{+5.64}_{-8.42}$ *E-09*	047 ± 3
369706	4666691	$2.98^{+1.41}_{-1.32}$ E-08	$-0.17^{+1.31}_{-1.34}$ *E-08*	035 ± 4
355563	4680833	1.91 ± 0.56E-08	*−0.39 ± 5.26E-09*	044 ± 4
341421	4694975	1.87 ± 0.43E-08	*−0.75 ± 3.92E-09*	042 ± 2
327279	4709117	2.23 ± 0.66E-09	*0.02 ± 6.00E-10*	056 ± 6
426274	4638406	1.04 ± 0.18E-08	*−0.78 ± 1.56E-09*	049 ± 2
412132	4652548	2.72 ± 0.68E-08	*−1.78 ± 6.13E-09*	049 ± 2
397990	4666691	1.41 ± 0.49E-08	*−1.51 ± 4.69E-09*	032 ± 3
383848	4680833	2.30 ± 0.82E-08	*−0.74 ± 7.97E-09*	053 ± 3
369706	4694975	2.64 ± 0.39E-08	*1.12 ± 3.43E-09*	028 ± 2
355563	4709117	8.94 ± 2.77E-09	*0.12 ± 2.65E-09*	046 ± 3
426274	4666691	8.51 ± 2.74E-09	−3.06 ± 2.57E-09	047 ± 2
397990	4694975	1.85 ± 0.68E-08	*1.40 ± 6.33E-09*	037 ± 6
383848	4709117	9.14 ± 1.43E-09	*0.14 ± 1.16E-09*	016 ± 2
369706	4723259	1.14 ± 0.28E-08	*−0.18 ± 2.47E-09*	055 ± 3

[a]The errors in the strain-rates within the Fucino Basin are asymmetrical (see Text S1). Strain-rates written in italics are those which have an absolute magnitude less than their error and thus the sign of the strain-rate is undetermined. The grid boxes are expressed in terms of the UTM coordinates of their mid points and all lie within UTM zone 33T.

Table 4. Table Comparing Maximum Horizontal Principal Strain-Rate Magnitudes and Directions Calculated Using Measurements of Striated Faults Offsetting Late Pleistocene and Holocene Features With Those Calculated From Summation of Moment Tensors Over a Time Period of 700 Years [*Selvaggi*, 1998]

Polygon	This Study Principal Strain-Rate hop $\dot{\varepsilon}_{11}$ ($\times 10^{-8}$ yr^{-1})	*Selvaggi* [1998] Principal Strain-Rate $\dot{\varepsilon}_{11}$ ($\times 10^{-8}$ yr^{-1})	This Study Principal Angle ψ (deg)	*Selvaggi* [1998] Principal Angle ψ (deg)
27	0.45 ± 0.10	0	052 ± 3	-
30	$2.03^{+0.12}_{-0.11}$	5.5 ± 1.7[a]	038 ± 1	041 ± 15
32	1.02 ± 0.13	0	043 ± 2	-
33	$1.40^{+0.39}_{-0.15}$	2.8 ± 0.8	045 ± 1	057 ± 15
35	0.51 ± 0.10	0	019 ± 3	-
36	$1.12^{+0.37}_{-0.10}$	1.4 ± 0.4	046 ± 1	042 ± 15
38	0.92 ± 0.10	0	048 ± 2	-

[a]The strain from the 2009 L'Aquila earthquake has been added to the result of *Selvaggi* [1998].

by geodetic site locations or seismic moment calculations facilitates comparison of different strain-rate data sets.

[39] *Anzidei et al.* [2005] report that the central Apennines Geodetic Network consisting of 125 temporary GPS stations distributed on 3–5 km average grid spacing, and set up since 1999, will soon be producing results. It appears that in the next few years it will be possible to directly compare strain-rates over a 15 ± 3 kyr time frame calculated in this study with those recorded over a few years on a scale that is smaller than the length scale of the faults responsible for the deformation. This will be a powerful combined database and should allow us to comment on the strain accumulation at timescales longer and shorter than individual seismic cycles and over length-scales comparable to the likely source dimensions (10–20 km) of damaging earthquakes in the central Apennines. It will facilitate identification of surpluses or deficits of elastic strain and coseismic earthquake strain compared to the longer-term multi-seismic cycle strains reported in this paper. This may identify areas that are candidates for impending earthquakes. It will also improve our knowledge of the spatial and temporal variability in the seismic cycle, because strain-rates from 15 ± 3 kyr provide information on the loading rates that can be used as yardsticks to assess the significance of shorter term strain-rates.

[40] In the meantime, prior to acquisition of GPS strains on a 3–5 km average grid spacing [*Anzidei et al.*, 2005], we can make some preliminary comments regarding regional strain accumulation, specific seismic hazards for smaller regions within the central Apennines, and the variability in the seismic cycle in the central Apennines.

[41] First, in terms of strain accumulation at a regional scale, strain-rates calculated on a 20 km × 20 km grid (Figure 4) and those in 5 km × 80 km bands crossing the Apennines (Figure 5), show a patch of extension centered on the Fucino plain, dying out along strike over a distance of c. 80 km both to the SE and NW. This patch of extension was noted by *Roberts and Michetti* [2004] and *Roberts* [2006], but does not appear to be resolved by published GPS or seismic moment summations. The patch of extension is located in an area containing a topographic bulge and a positive free-air gravity anomaly, as noted by *D'Agostino et al.* [2001b, Figures 3 and 5] (Figure 4). They suggested these anomalies were dynamically-supported by mantle convection. The geographic coincidence of the patch of extension we describe and the topographic and gravity anomalies are consistent with the ideas of *D'Agostino et al.* [2001b] that "mantle upwelling beneath the central Apennines has been the dominant geodynamic process during the Quaternary, controlling both the geomorphic evolution and distribution of active deformation"; "the active extension may be more closely related to ongoing sub-crustal processes than to the relative motions of the surrounding lithospheric blocks within the Mediterranean collision zone". Note that individual faults, such as those within areas that at first sight appear to have complicated fault geometries (e.g. Polygon K in Figure 4; compare with Figure 3), appear to be working together to achieve the strain-rate field evident at a larger scale, such as the systematic decrease in strain-rates both along strike and across strike away from the Fucino Plain observed with a 20 km × 20 km grid size (Figure 4). Fault interaction of this kind has also been observed across the Taupo Rift, New Zealand [*Nicol et al.*, 2006] and in Southern California [*Dolan et al.*, 2007]. Thus, the slip-rates on individual faults are not random, but are interacting in such a

Table 5. Table Comparing the Shear Strain-Rates Calculated Using Measurements of Striated Faults Offsetting Late Pleistocene and Holocene Features With Those Calculated From GPS Reoccupation of a Triangulation Network Over a Time Period of 126 Years [*Hunstad et al.*, 2003][a]

Polygon	This Study Shear Strain γ_1 ($\times 10^{-8}$ yr^{-1})	*Hunstad et al.* [2003] Shear Strain γ_1 ($\times 10^{-8}$ yr^{-1})	This Study Shear Strain γ_2 ($\times 10^{-8}$ yr^{-1})	*Hunstad et al.* [2003] Shear Strain γ_2 ($\times 10^{-8}$ yr^{-1})	This Study Principal Angle ψ (deg)	*Hunstad et al.* [2003] Principal Angle ψ (deg)
2	$0.71^{+0.07}_{-0.06}$	*0.37 ± 2.9*	0.07 ± 0.03	−3.8 ± 2.4	042 ± 1	092 ± 42
3	$0.70^{+0.13}_{-0.08}$	*1.8 ± 2.6*	0.18 ± 0.05	3.7 ± 2.7	038 ± 2	018 ± 33
4	0.26 ± 0.04	−3.8 ± 2.9	0.03 ± 0.02	5.2 ± 2.4	042 ± 2	077 ± 22
7	0.95 ± 0.07	11.6 ± 3.2	0.15 ± 0.07	*−1.9 ± 2.8*	039 ± 2	054 ± 7
8	$1.72^{+0.39}_{-0.11}$	5.8 ± 3.0	$-0.12^{+0.08}_{-0.06}$	*0.5 ± 2.9*	046 ± 1	052 ± 15
12	0.29 ± 0.04	−4.0 ± 3.0	0.11 ± 0.04	−2.8 ± 2.7	035 ± 3	032 ± 25

[a]Strain-rates written in italics are those which have an absolute magnitude less than their error and thus the sign of the strain-rate is undetermined.

way as to accommodate forces associated with the regional boundary conditions.

[42] Second, we note that strain-rates measured over 15 ± 3 kyr are in places lower than those measured over time periods that are similar to or shorter than likely seismic cycle durations (e.g. 700 years of seismicity, Figure 6 Polygons 30 and 33; 126 years of geodetic strain, Figure 7); elsewhere, strain-rates measured over 15 ± 3 kyr are higher (e.g. 700 years of seismicity, Figure 6, Polygons 32, 35 and 38). We have not determined the explanation for this in this paper, but discuss it in any case. One explanation for why the 126 year geodetic strain-rates are higher than those for 15 ± 3 kyr could involve temporal variability in the rate of interseismic elastic strain accumulation; we speculate that this could occur over 2 time scales. (1) Within a single seismic cycle, the interseismic elastic strain-rates may change approaching failure or after failure due to non-linear stress (time varying stress) versus strain relationships associated with temporal changes in the magnitude-frequency relationship of seismicity (b-value); such non-linearity prior to failure is well-known from rock-deformation experiments (see *Sammonds et al.* [1992] and *Main* [1996] for a review), and, if applicable at the scale of the active faults we study, it is unclear what effect large earthquakes like the 1915 Ms 6.9 Fucino earthquake will have had on the 126 year geodetic strain-rates. (2) Over timescales involving multiple seismic cycles, if large earthquakes are clustered in time, the preparation time for each earthquake is shorter than that for earthquakes outside this temporal cluster. In other words, the time period over which stress increases from post-failure levels to the failure stress will be shorter for shorter recurrence intervals. Paleoseismic data suggest that this can be the case as measured recurrence intervals change through time on individual faults [*Palumbo et al.*, 2004]. Measured rates of interseismic elastic strain from GPS may thus be anomalously high compared to the mean interseismic rates measured over a time period long enough to contain both temporal clusters and anticlusters of large earthquakes. Both of the above factors could explain why interseismic strain-rates can be higher or lower than those measured over multiple earthquake cycles. Another factor to consider is that of the mis-location of historical earthquakes. For example, one of the three 9th September 1349 A.D. earthquakes caused intensity IX–X shaking in the Salto Valley (Figure 1) and was probably a Me 6.3 earthquake [*Guidoboni et al.*, 2007]. We suggest this earthquake may have ruptured the Fiamignano Fault in the Salto Valley so its moment release should be included in Polygon 32 Figure 6 [*Guerrieri et al.*, 2002]. However, it appears that *Selvaggi* [1998] has included the strain from this earthquake in Polygon 30 rather than Polygon 32. This may also be true of Polygon 36 and 38 if another of the three 9th September 1349 A.D. (Me 6.7) earthquakes ruptured the Cassino Fault (although see *Galli and Naso* [2009]), and the SE end of the Liri fault was ruptured by the 1654 A.D. earthquake (Me 6.1). The strain from these earthquakes appears to have been assigned to Polygons 33 and 36 by *Selvaggi* [1998]. If the above is incorrect and *Selvaggi* [1998] has correctly assigned coseismic strain to polygons, we note deficits in coseismic strain in the order of $(0.5–1) \times 10^{-2}$ ppm/yr in Polygons 32, 35 and 38, equivalent to about 2 (2.3), 1 (0.5) and 2 (1.7) earthquakes respectively with 1 m of dip slip and rupture lengths of 15 km on fault planes dipping at 60° in 700 yrs. We note that the strain-rate calculated from summation of moment tensors in polygon 30 was higher than that for the long-term (15 ± 3 kyrs) rate prior to the 6th April 2009 L'Aquila Earthquake (Mw 6.3). The L'Aquila earthquake contributes only $0.4 \pm 0.2 \times 10^{-2}$ ppm/yr (7% of the seismic strain stated) given that it produced 0.6–0.8 m of slip over a length of 12 km [*Walters et al.*, 2009]. If the pre-2009 earthquakes studied by *Selvaggi* [1998] are located correctly within polygon 30, then the L'Aquila earthquake occurred in a location where no strain deficit existed, and may thus represent an example of seismicity that is clustered in time to an extent greater than that expected of the long-term slip-rate on the fault. Alternatively, if *Selvaggi* [1998] has used an incorrect location for the 1349 (Me 6.3) event, which was, instead, located in Polygon 32 (see earlier text), then the strain-rates implied by seismicity including the 2009 L'Aquila earthquake more closely match the long-term (15 ± 3 kyrs) strain-rates. Clearly, it is very important for future research to focus on exactly which polygons contained the aforementioned large magnitude historical earthquakes, and specifically, which faults ruptured.

[43] It is noteworthy that another possible explanation as to why the strain-rates measured using geodesy and seismic moment summation are greater than geologically inferred strain-rates, particularly strain-rates orthogonal to the regional extension direction, is that there could be strain between the observed faults and thus by measuring strain-rates using offsets across fault scarps some of the strain at the surface that has accumulated over 15 ± 3 kyrs has been missed; in this scenario, the differences between the strain-rates measured using geodesy and across fault scarps could be used as a measure of the strain between faults. There could perhaps be strain produced by faults at depth that do not break the surface or only have surface offsets of less than a few meters. There could also perhaps be strain produced by events during which surface ruptures do not occur on distinct fault planes but rather as offsets in the hanging wall of the main fault plane, as these small offsets will erode with time, it is possible that by measuring the offsets of the fault scarps several events have been missed. Such strains would have to be larger than the strains accommodated on the faults that have broken the surface if the long-term 10^4 yr strain-rates are to match the 10^{1-2} yr strain-rates implied by historical earthquakes and geodesy. However, we feel that this is unlikely as: (1) Strains on small faults around major faults, where measured from inactive faults elsewhere, are known to accommodate a maximum of a few tens of percent of the strains associated with the major faults [*Scholz and Cowie*, 1990; *Walsh et al.*, 1991]; (2) all historical earthquakes in the central Italian Apennines have been accounted for on the major faults, with almost all known historical earthquakes identified during paleoseismic trench investigations (see *Galli et al.* [2008] for a review) and the remaining events' recorded damage locations being consistent with those expected of earthquakes on known major faults that have not had paleoseismic trench investigations along them [e.g., *Guerrieri et al.*, 2002]; and (3) the microseismicity in the last c. 30 years does not show widespread activity on lots of small faults that might have slip-rates much less than 0.1 mm/yr, but rather small bursts of activity on mapped major faults. However for the present, due to the above uncertainties concerning rates of elastic strain accumulation and earthquake locations, the fact remains

that we are unsure of how to interpret the differences between 10^2 yr and 10^4 yr strain-rates in terms of impending seismic hazard, and this is an avenue for future work.

[44] Third, our method allows us to calculate fault-specific earthquake recurrence intervals for given magnitudes, and thus comment on earthquake/fault interactions. The strain-rates on the 5 km × 5 km grid can be converted into earthquake frequencies for a given earthquake magnitude so we can map how fault-specific earthquake recurrence intervals vary along individual faults and between faults (Figure 8). For a given magnitude, say a 1 m pure dip-slip earthquake, we calculate the number of earthquakes that should have occurred in 15 ± 3 kyr within 5 km × 5 km grid squares containing known fault lengths by dividing the principal horizontal strain by the principal horizontal strain released in each earthquake (Figure 8). Note that different earthquake recurrence estimates would be derived for different assumptions regarding the slip distribution and magnitude. The implied fault-specific earthquake recurrence intervals vary from 400 years to as long as 7300 years (Table 6). We can check whether such recurrence intervals are realistic through comparison with paleoseismological results. For example, trench investigations along the Fucino fault show that there have been 3 large earthquakes in the last 2000 yrs in the center of the fault near San Benedetto dei Marsi [*Michetti et al.*, 1996], only 2 nearer the SE tip of the fault between Venere and Gioia dei Marsi [*Galadini and Galli*, 1999], and only 1 at the NW tip along the Ovindoli-Pezza segment [*Pantosti et al.*, 1996]. We estimate fault-specific recurrence intervals of 750 yrs, 1050 yrs and 2300 yrs at these sites (Figure 8), consistent with the paleoseismic data. Our work thus highlights that a change in the recurrence interval for a given magnitude earthquake is expected along a fault because strain-rates change over this length scale. Hence this reconciles the spatial distribution of paleoseismic trench results at different sites along a given fault. Cl^{36} cosmogenic exposure dating of surface slip events on the Velino-Magnola Fault shows there have been between 5 and 7 earthquakes in the last 12 kyrs [*Palumbo et al.*, 2004], suggesting a recurrence interval of 1700–3000 yrs; in the same grid square we estimate a recurrence interval of 2750 yrs (Figure 8). Thus the fault-specific recurrence intervals implied by our calculations produce a similar spatial variation in the occurrence of large magnitude earthquakes to that recorded by paleoseismological observations. Note also that the implied recurrence intervals also vary between different faults and this may allow us to identify deficits of slip in large magnitude earthquakes. The Sulmona and Liri Faults have implied fault-specific recurrence intervals of less than 600 years and the Pescasseroli Fault has an implied fault-specific recurrence interval of less than 800 yrs yet none of these faults have ruptured in a large magnitude (<Ms 6.0) earthquake since 1349 A.D., and perhaps for over 1000 years. Also paleoseismological data for the Campo Imperatore Fault shows that it has not ruptured for over 2000 years [*Galli et al.*, 2002]; its implied fault specific recurrence interval is 650 yrs (Table 6). Despite this, we note that strain-rates implied by historical seismic moment release in the polygons containing these faults (Polygons 30, 33 and 36; Figure 6) is higher than that implied by 15 ± 3 kyr fault slip-rates if earthquakes have been assigned to the correct polygons by *Selvaggi* [1998]. Perhaps the >Ms 6.0 earthquakes of 1349 A.D. on the Cinque-Miglia Fault, 1915 A.D. on the Fucino Fault, and 1461 A.D., 1762 A.D. and 2009 A.D. on the L'Aquila Fault and its immediate neighbors, have released more strain during the last 700 yrs than expected from the 15 ± 3 kyr strain-rate and have delayed slip on the Sulmona, Pescasseroli, Campo Imperatore and Liri Faults. This implies interaction between the faults that have ruptured and those that have not within each of the polygons. This type of observation may help to identify candidates for the location of the next large magnitude earthquake in the central Apennines. The implied temporal clustering of large magnitude earthquakes due to interaction is consistent with the fact that Cl^{36} dating has shown that coseismic slip events can be clustered in time [*Palumbo et al.*, 2004]. It may also be consistent with the observation that paleoseismic results show that faults appear to be able to share strain over a given time period, that is, the faults are interacting. For example, for grid square K in Figure 4 containing the Velino-Magnola, Tre-Monti, Ovindoli-Pezza and Campo Felice Faults, the 15 kyr loading rate results in a strain-rate of $0.030^{+0.014}_{-0.013}$ ppm/yr. This rate is not anomalous compared to grid squares located along strike that have experienced large magnitude earthquakes in the last 4500 years (grid square J which contains the 1915 A.D. Ms 6.9 Avezzano earthquake and grid squares L and M which probably contain the 1349 A.D. Me 6.3 earthquake) or grid squares across strike (grid squares E and S). Thus, we can conclude that the lack of earthquakes on the Velino-Magnola fault in the last 4500 years [*Palumbo et al.*, 2004] measured with cosmogenic exposure dating is not due to a lack of loading over this time period. Strain in the last 4500 years in grid square K presumably results from a combination of earthquakes on the Tre-Monti, Ovindoli-Pezza and Campo Felice Faults [see *Pantosti et al.*, 1996], counteracting the slip-rate deficit on the Velino fault. Thus, interaction between faults [*Cowie and Roberts*, 2001], where they share the strain over given time periods, is a plausible explanation for why earthquakes are clustered in time on specific faults. Although Figure 8 is useful in that it shows the long-term rate of implied fault-specific earthquake recurrence intervals, the natural variation in fault-specific earthquake recurrence intervals, usually expressed as the coefficient of variation in seismic hazard determinations [*Savage*, 1992; *Toda et al.*, 1995; *Ellsworth et al.*, 1999; *Parsons et al.*, 2000], must also be considered. Longer paleoseismic records are perhaps the only way to test whether fault interaction does control the longevity and intensity for clusters of large magnitude earthquakes.

[45] This leads to the question of how long a slip-rate record is needed to average out temporal earthquake clustering and gain the long-term strain-rate field. We note that we have not proved that 12–18 kyrs is a long enough time period to average out the effects of temporal clusters and anticlusters. However, we think there are two reasons why 12–18 kyrs may approach a long enough time period. First, *Roberts et al.* [2004] calculated slip-rates on faults in the central Apennines needed to satisfy scaling relationships between the lengths and displacements on faults that develop over millions of years. They found that these calculated slip-rates were consistent with slip-rates measured over 12–18 kyrs reported by *Roberts and Michetti* [2004]. This suggests to us that 12–18 kyrs may well be a long enough time period to average strain-rates over temporal clusters and anticlusters. Second, the correspondence between the patch of extension we have measured on our

Table 6. Implied Recurrence Intervals for Each Fault[a]

Fault	Recurrence Interval (years)
Liri	400
Sulmona	550
Fucino	550
Campo Imperatore	650
Pescasseroli	800
Trasacco	850
Fiamignano	850
Maiella	850
L'Aquila	900
Laga	1150
Pettino	1250
Barete	1400
Velino-Magnola	1550
Aremogna-Cinque Miglia	1650
Scurcola	1750
Parasano-Pescina	1850
Carsoli	1850
Assergi	1900
Cassino	2050
Roccapreturo	2150
Sella di Corno	2250
Monte Christo	2300
Leonessa	2800
San Sebastiano	2950
Rieti	3200
Campo Felice	3600
Ocre	3800
Pescocostanzo	4600
Ventrino	6650
Tre Monti	7300

[a]The only values shown in the table are from the 5 km grid squares with the minimum recurrence intervals calculated for each fault.

20 km × 20 km grid and the topographic and free-air gravity anomalies described by *D'Agostino et al.* [2001b] suggest that the 15 kyrs strain-rate field at a 20 km × 20 km grid scale relates to the far field driving forces rather than to shorter term interactions between faults associated with transient rates of strain accumulation; thus we suggest that the strains in the 20 km × 20 km grid describe the long-term multi-seismic-cycle strain-rate field. A test of this would be to compare the strain-rates calculated over 12–18 kyrs with those measured on a longer time-period (10^{5-6} yr) [*Friedrich et al.*, 2003; *Mouslopoulou et al.*, 2009]. However, this is beyond the scope of this paper, and awaits identification of geological offsets older than 12–18 ka that can be mapped across the central Apennines [*Blumetti and Guerrieri*, 2007]. However, despite this, we believe that the strain-rates we have presented averaged over 12–18 kyrs provide important new insights into the deformation and the significance of strain-rates measured over shorter time periods via geodesy and seismic moment summations; such long-term strain-rates must be included in reasoning that attempts to identify deficits in earthquake strain for seismic hazard assessments.

6. Conclusions

[46] Strain-rates averaged over 15 ± 3 kyrs in the central Apennines can be constructed from measurements of striated faults offsetting Late Pleistocene and Holocene features. These allow a view of the multi-seismic cycle deformation. Calculating strain-rates within a regular square grid allows comparison with other results calculated over areas with various sizes and geometries, and over time periods of interseismic elastic strain, or time periods containing a single large magnitude earthquake and some interseismic elastic strain. Strain-rates calculated over 15 ± 3 kyrs within 5 km × 5 km grid squares vary from zero up to $2.34 \pm 0.54 \times 10^{-7}$ yr^{-1} and resolve variations in strain orientations and magnitudes along the strike of individual faults, comparable with the source dimensions of damaging earthquakes (10–40 km). When integrated over an area of 80 km × 160 km, horizontal strain-rates within the central Apennines are $1.18^{+0.12}_{-0.04} \times 10^{-8}$ yr^{-1} and $-1.83^{+3.80}_{-4.43} \times 10^{-10}$ yr^{-1} parallel and perpendicular to the regional principal strain direction (043°–223° ± 1°), consistent with extension rates of $\leq 3.1^{+0.8}_{-0.4}$ mm yr^{-1} calculated in 5 km × 80 km boxes crossing the strike of the central Apennines. Although broadly comparable in direction to strain-rates calculated using geodesy (126 yrs, 11 yrs and 5 yrs) and seismic moment summation (710 yrs, a time period extended to include the 2009 Mw 6.3 L'Aquila earthquake), the magnitude of the strain-rate is about 2.6 × less over a comparable area. Smaller areas (≈2000 km^2), corresponding to polygons defined by geodesy campaigns and seismic moment summations, show higher 10^2 yr strain-rates than 10^4 yr strain-rates, or the opposite situation depending on the area studied. This demonstrates that strain-rates vary spatially on the length-scale of individual active faults and on a timescale between 10^2 yr and 10^4 yr in the central Apennines. The 15 ± 3 kyr strain-rates suggest that extension is concentrated in a patch coincident with anomalously high topography and free-air gravity, consistent with the idea that sub-crustal processes may dominate the deformation in the central Apennines rather than forces associated with plate boundaries. The 15 ± 3 kyr strain-rates imply fault specific earthquake recurrence intervals that are consistent with palaeoseismological data, and in the range of a few hundred years to several thousand years. Overall, strain-rates averaged over 15 ± 3 kyrs in the central Apennines are available at a higher spatial resolution than strain-rates derived from existing geodetic and earthquake moment summations, and provide a multi-seismic-cycle view of the deformation. They provide new insights into temporal and spatial variations in strain-rates associated with the occurrence of large magnitude, damaging earthquakes, that palaeoseismological data prove are clustered in time.

[47] **Acknowledgments.** This study was funded by a studentship to J.P. Faure Walker (NER/S/A/2006/14042) and NERC grants NE/E01545X/1, NE/B504165/1 and GR9/02995. We thank Alessandro Michetti, Ioannis Papanikolaou, Nigel Morewood, Richard Phillips, Alex Whittaker, Greg Tucker, Mikael Attal, Kerry Sieh, Eutizio Vittori, Romilly Everett, Martyn Race, Tim Wright, Anna-Maria Blumetti, and Luca Guerrieri for discussions and help during the fieldwork. We thank Andy Nicol, John Walsh, and an anonymous reviewer for their comments which helped improve the manuscript.

References

Allen, J., et al. (1999), Rapid environmental changes in southern Europe during the last glacial period, *Nature*, *400*, 740–743.

Anderson, H., and J. Jackson (1987), Active tectonics of the Adriatic region, *Geophys. J. Int.*, *91*(3), 937–983.

Anzidei, M., P. Baldi, A. Pesci, A. Esposito, A. Galvani, F. Loddo, P. Cristofoletti, A. Massucci, and S. Del Mese (2005), Geodetic deformation across the central Apennines from GPS data in the time span 1999–2003, *Ann. Geophys.*, *48*(2), 259–271.

Armijo, R., H. Lyon-Caen, and D. Papanastassiou (1992), East-west extension and Holocene normal-fault scarps in the Hellenic arc, *Geology*, *20*, 491–494.

Basili, R., G. Valensise, P. Vannoli, P. Burrato, U. Fracassi, S. Mariano, M. M. Tiberti, and E. Boschi (2008), The Database of Individual Seismogenic Sources (DISS), version 3: Summarizing 20 years of research on Italy earthquake geology, *Tectonophysics*, *453*(1–4), 20–43.

Blumetti, A. M., and L. Guerrieri (2007), Fault-generated mountain fronts and the identification of fault segments: Implications for seismic hazard assessment, *Boll. Soc. Geol. Ital.*, *126*(2), 307–322.

Boschi, E., G. Ferrari Gasperini, P. E. Guidoboni, G. Smriglio, and G. Valensise (1995), *Catalogo dei forti terremoti in Italia dal 461 A.C. al 1980*, 973 pp., Inst. Naz. Geofis., Rome.

Bull, J. M., P. M. Barnes, G. Lamarche, D. J. Sanderson, P. A. Cowie, S. K. Taylor, and J. K. Dix (2006), High-resolution record of displacement accumulation on an active normal fault: Implications for models of slip accumulation during repeated earthquakes, *J. Struct. Geol.*, *28*, 1146–1166.

Cavinato, G. P., and P. G. De Celles (1999), Extensional basins in the tectonically bimodal central Apennines fold-thrust belt, Italy: Response to corner flow above a subducting slab in retrograde motion, *Geology*, *27*(10), 955–958.

Clarke, P. J., et al. (1998), Crustal strain in central Greece from repeated GPS measurements in the interval 1989–1997, *Geophys. J. Int.*, *135*, 195–214.

Cowie, P. A. (1998), A healing-reloading feedback control on the growth rate of seismogenic faults, *J. Struct. Geol.*, *20*(8), 1075–1087.

Cowie, P. A., and G. P. Roberts (2001), Constraining slip rates and spacings for active normal faults, *J. Struct. Geol.*, *23*, 1901–1915.

D'Addezio, G., E. Masana, and D. Pantosti (2001), The Holocene paleoseismicity of the Aremogna-Cinque Miglia Fault (central Italy), *J. Seismol.*, *5*, 181–205.

D'Agostino, N., R. Giuliani, M. Mattone, and L. Bonci (2001a), Active crustal extension in the central Apennines (Italy) inferred from GPS measurements in the interval 1994–1999, *Geophys. Res. Lett.*, *28*(10), 2121–2124.

D'Agostino, N., J. Jackson, F. Dramis, and R. Funiciello (2001b), Interactions between mantle upwelling, drainage evolution and active normal faulting: An example from the central Apennines (Italy), *Geophys. J. Int.*, *147*, 475–497.

Davies, R., P. England, B. Parsons, H. Billiris, D. Paradissis, and G. Veis (1997), Geodetic strain of Greece in the interval 1892–1992, *J. Geophys. Res.*, *102*(B11), 24,571–24,588.

Doglioni, C. (1993), Some remarks on the origin of foredeeps, *Tectonophysics*, *228*, 1–20.

Dolan, J., D. Bowman, and C. Sammis (2007), Long-range and long-term fault interactions in southern California, *Geology*, *35*, 855–858.

Ellsworth, W. L., M. V. Matthews, R. M. Nadeau, S. P. Nishenko, P. A. Reasenberg, and R. W. Simpson (1999), A physically-based earthquake recurrence model for estimation of long-term earthquake probabilities, *U.S. Geol. Surv. Open File Rep.*, *99–522*.

England, P., and P. Molnar (1997), The field of crustal velocity in Asia calculated from Quaternary rates of slip on faults, *Geophys. J. Int.*, *130*, 551–582.

Friedrich, A. M., B. P. Wernicke, N. A. Niemi, R. A. Bennett, and J. L. Davis (2003), Comparison of geodetic and geologic data from the Wasatch region, Utah, and implications for the spectral character of Earth deformation at periods of 10 to 10 million years, *J. Geophys. Res.*, *108*(B4), 2199, doi:10.1029/2001JB000682.

Fung, Y. C. (1977), *A First Course in Continuum Mechanics*, Prentice-Hall, Englewood Cliffs, N. J.

Galadini, F., and P. Galli (1999), The Holocene paleoearthquakes on the 1915 Avezzano earthquake faults (central Italy): Implications for active tectonics in the central Apennines, *Tectonophysics*, *308*, 143–170.

Galadini, F., and P. Galli (2000), Active tectonics in the central Apennines (Italy): Input data for seismic hazard assessment, *Nat. Hazards*, *22*, 225–270.

Galadini, F., and P. Galli (2003), Paleoseismology of silent faults in the central Apennines (Italy): the Mt. Vettore and Laga Mts. Faults, *Ann. Geophys.*, *46*, 815–836.

Galadini, F., P. Galli, and C. Giraudi (1997), Geological Investigations of Italian earthquakes: new paleoseismological data from the Fucino Plain (central Italy), *J. Geodyn.*, *24*, 87–103.

Galli, P. A. C., and J. A. Naso (2009), Unmasking the 1349 earthquake source (southern Italy): palaeoseismological and archaeoseismological indications from the Aquae Iuliae fault, *J. Struct. Geol.*, *31*, 128–149.

Galli, P., F. Galadini, M. Moro, and C. Giraudi (2002), New paleoseismological data from the Gran Sasso d'Italia area (central Apennines), *Geophys. Res. Lett.*, *29*(7), 1134, doi:10.1029/2001GL013292.

Galli, P., F. Galadini, and D. Pantosti (2008), Twenty years of paleoseismology in Italy, *Earth Sci. Rev.*, *88*, 89–117.

Giraudi, C., and M. Frezzotti (1986), Inversione pleistocenica del drenaggio in alta Val Roveto (Abruzzo sud occidentale), *Mem. Soc. Geol. Ital.*, *35*, 847–853.

Giraudi, C., and M. Frezzotti (1995), Palaeoseismicity in the Gran Sasso massif (Abruzzo, central Italy), *Quat. Int.*, *25*, 81–93.

Giraudi, C., and M. Frezzotti (1997), Late Pleistocene glacial events in the central Apennines, Italy, *Quat. Res.*, *48*, 280–290.

Guerrieri, L., F. Pascarella, S. Silvestri, and L. Serva (2002), Evoluzione recente del paesaggio e dissesto geologico-idraulico: Primi risultati in un'area campione dell'Appennino Centrale (valle del Salto-Rieti), *Mem. Soc. Geol. Ital.*, *507*, 453–461.

Guidoboni, E., G. Ferrari, D. Mariotti, A. Comastri, G. Tarabusi, and G. Valensise (2007), *CFTI4Med, Catalogue of Strong Earthquakes in Italy (461 B.C.-1997) and Mediterranean Area (760 B.C.-1500)*, Inst. Naz. Geofis., Rome. (Available from http://storing.ingv.it/cfti4med/.)

Haines, A. J., and W. E. Holt (1993), A procedure for obtaining the complete horizontal motions within zones of distributed deformation from the inversion of strain-rate data, *J. Geophys. Res.*, *98*(B7), 12,057–12,082.

Holt, W. E., and A. J. Haines (1995), The kinematics of northern South Island, New Zealand, determined from geologic strain-rates, *J. Geophys. Res.*, *100*(B9), 17,991–18,010.

Hunstad, I., G. Selvaggi, N. D'Agostino, P. England, P. Calrke, and M. Pierozzi (2003), Geodetic strain in peninsular Italy between 1875 and 2001, *Geophys. Res. Lett.*, *30*(4), 1181, doi:10.1029/2002GL016447.

Jackson, J., A. Gagnepain, A. Houseman, J. King, G. Papadimitriou, G. C. P. Soufliers, and C. Virieux (1982), Seismicity, normal faulting, and the geomorphological development of the Gulf of Corinth (Greece): The Corinth earthquakes of February and March 1981, *Earth Planet. Sci. Lett.*, *57*, 377–397.

Kostrov, V. V. (1974), Seismic moment and energy of earthquakes, and seismic flow of rock, *Izv. Earth Phys.*, *1*, 23–40. (Engl. Transl. UDC 550.341, 13–21.)

Kreemer, C., N. Chamot-Rooke, and X. Le Pichon (2004), Constraints on the evolution and vertical coherency of deformation in the northern Aegean from a comparison of geodetic, geologic and seismologic data, *Earth Planet. Sci. Lett.*, *225*, 329–346.

Main, I. G. (1996), Statistical physics, seismogenesis, and seismic hazard, *Rev. Geophys.*, *34*(4), 433–462.

Maniatis, G., and A. Hampel (2008), Along-strike variations of the slip direction on normal faults: Insights from three-dimensional finite-element models, *J. Struct. Geol.*, *30*, 21–28.

Margottini, C., and A. Screpanti (1998), Temporal evolution of the seismic crisis related to the 13th January 1915, Avezzano earthquake, Historical seismicity of central-eastern mediterranean region, in *Proceedings of the 1987 ENEA-IAEA International Workshop*, edited by C. Margottini and L. Serva, pp. 185–193, Ital. Natl. Agency for New Technol. Energy and Sustainable Econ. Dev., Rome.

Michetti, A. M., F. Brunamonte, L. Serva, and E. Vittori (1996), Trench investigations of the 1915 Fucino earthquake fault scarps (Abruzzo, central Italy): Geological evidence of large historical events, *J. Geophys. Res.*, *101*(B3), 5921–5936.

Michetti, A. M., L. Ferreli, E. Esposito, S. Porfido, A. M. Blumetti, E. Vittori, L. Serva, and G. P. Roberts (2000), Ground effects during the 9 September 1998, Mw = 5.6, Lauria Earthquake and the seismic potential of the aseismic Pollino region in southern Italy, *Seismol. Res. Lett.*, *71*, 31–46.

Miller, A. S., C. Collettini, L. Chiaraluce, M. Cocco, M. Barchi, and B. J. P. Kaus (2004), Aftershocks driven by a high-pressure CO2 source at depth, *Nature*, *427*, 724–727.

Molnar, P. (1983), Average regional strain due to slip on numerous faults of different orientations, *J. Geophys. Res.*, *88*, 6430–6432.

Montone, P., A. Amato, and S. Pondrelli (1999), Active stress map of Italy, *J. Geophys. Res.*, *104*, 25,595–25,610.

Morewood, N. C., and G. P. Roberts (1999), Lateral propagation of the surface trace of the South Alkyonides normal fault segment, central Greece: Its impact on models of fault growth and displacement-length relationships, *J. Struct. Geol.*, *21*(6), 635–652.

Morewood, N. C., and G. P. Roberts (2000), The geometry, kinematics and rates of deformation within an en echelon normal fault boundary, central Italy, *J. Struct. Geol.*, *22*, 1027–1047.

Moro, M., V. Bosi, F. Galadini, P. Galli, B. Giaccio, P. Messina, and A. Sposato (2002), Analisi paleosismologiche lungo la faglia del M. Marine (alta valle dell'Aterno): Risultati preliminari, Il Quat., *Ital. J. Quat. Sci.*, *15*, 259–270.

Mouslopoulou, V., J. J. Walsh, and A. Nicol (2009), Fault displacement rates on a range of timescales, *Earth Planet. Sci. Lett.*, *278*, 186–197.

Nicol, A., J. Walsh, K. Berryman, and P. Villamor (2006), Interdependence of fault displacement rates and paleoearthquakes in an active rift, *Geology*, *34*, 865–868.

Palumbo, L., L. Benedetti, D. Bourles, A. Cinque, and R. Finkel (2004), Slip history of the Magnola fault (Apennines, central Italy) from ^{3}6Cl surface exposure dating: evidence for strong earthquakes over the Holocene, *Earth Planet. Sci. Lett.*, *225*, 163–176.

Pantosti, D., G. D'Addezio, and F. Cinti (1996), Paleoseismicity of the Ovindoli-Pezza fault, central Apennines, Italy: A history including a large, previously unrecorded earthquake in the Middle Ages (860–1300 A.D.), *J. Geophys. Res.*, *101*, 5937–5960.

Papanikolaou, I. D., G. P. Roberts, and A. M. Michetti (2005), Fault scarps and deformation rates in Lazio-Abruzzo, central Italy: Comparison between geological fault slip-rate and GPS data, *Tectonophysics*, *408*, 147–176.

Parsons, T., S. Toda, R. S. Stein, A. Barka, and J. Dieterich (2000), Heightened odds of large earthquakes near Istanbul: An interaction- based probability calculation, *Science*, *288*(5466), 661–665.

Patacca, E., R. Sartori, and P. Scandone (1990), Tyrrhenian Basin and Apenninic Arcs: Kinematic relations since late Tortonian times, *Mem. Soc. Geol. Ital.*, *45*, 425–451.

Piccardi, L., Y. Gaudemer, P. Tapponnier, and M. Boccaletti (1999), Active oblique extension in the central Apennines (Italy): Evidence from the Fucino region, *Geophys. J. Int.*, *139*, 499–530.

Pizzi, A., and G. Pugliese (2004), InSAR-DEM analyses integrated with geologic field methods for the study of long-term seismogenic fault behavior: Applications in the axial zone of the central Apennines (Italy), *J. Seismol.*, *8*, 313–329.

Pondrelli, S., A. Morelli, and E. Boschi (1995), Seismic deformation in the Mediterranean area estimated by moment tensor summation, *Geophys. J. Int.*, *122*(3), 938–952.

Postpischl, D. (Ed.) (1985), *Atlas of Isoseismal Maps of the Italian Earthquakes*, 164 pp., Cons. Naz. Ric. Quad. Ric. Sci., Rome.

Roberts, G. P. (1996), Variation in fault slip directions along active and segmented normal fault systems, *J. Struct. Geol.*, *18*, 835–845.

Roberts, G. P. (2006), Multi seismic cycle velocity and strain fields for an active normal fault system, central Italy, *Earth Planet. Sci. Lett.*, *251*, 44–51.

Roberts, G. P. (2007), Fault orientation variations along the strike of active normal fault systems in Italy and Greece: Implications for predicting the orientations of subseismic-resolution faults in hydrocarbon reservoirs, *AAPG Bull.*, *91*(1), 1–20.

Roberts, G. P. (2008), Visualisation of active normal fault scarps in the Apennines, Italy: A key to assessment of tectonic strain release and earthquake rupture, *Google Earth Sci. J. Virtual Explor.*, *29*, paper 4, doi:10.3809/jvirtex.2008.00197.

Roberts, G. P., and A. M. Michetti (2004), Spatial and temporal variations in growth rates along active normal fault systems: an example from the Lazio-Abruzzo Apennines, central Italy, *J. Struct. Geol.*, *26*, 339–376.

Roberts, G. P., A. M. Michetti, P. Cowie, N. C. Morewood, and I. Papanikolaou (2002), Fault slip-rate variations during crustal-scale strain localisation, central Italy, *Geophys. Res. Lett.*, *29*(8), 1168, doi:10.1029/2001GL013529.

Roberts, G. P., P. Cowie, I. Papanikolaou, and A. M. Michetti (2004), Fault scaling relationships, deformation rates and seismic hazards: an example from the Lazio-Abruzzo Apennines, central Italy, *J. Struct. Geol.*, *26*, 377–398.

Salvi, S., F. R. Cinti, L. Colini, G. D'Addezio, F. Doumaz, and E. Pettinelli (2003), Investigation of the active Celano-L'Aquila Fault System, Abruzzi (central Apennines, Italy) with combined ground penetrating radar and palaeoseis- mic trenching, *Geophys. J. Int.*, *155*, 805–818.

Sammonds, P. R., P. G. Meredith, and I. G. Main (1992), Role of pore fluids in the generation of seismic precursors to shear fracture, *Nature*, *359*, 228–230.

Savage, J. C. (1992), The uncertainty in earthquake conditional probabilities, *Geophys. Res. Lett.*, *19*, 709–712.

Schlagenhauf, A. (2009), Identification des forts seismes passes sur les failles normales actives de la region Lazio-Abruzzo (Italie centrale) par cosmogeniques (36Cl) de leurs escarpments, Ph.D. thesis, Univ. Joseph Fourier, Grenoble, France.

Scholz, C. H., and P. A. Cowie (1990), Determination of total strain from faulting using slip measurements, *Nature*, *346*, 837–839.

Selvaggi, G. (1998), Spatial distribution of horizontal seismic strain in the Apennines from historical earthquakes, *Ann. Geofis.*, *41*(2), 241–251.

Serpelloni, E., M. Anzidei, P. Baldi, G. Casula, and A. Galvani (2005), Crustal velocity and strain-rate fields in Italy and surrounding regions: New results from the analysis of permanent and non-permanent GPS networks, *Geophys. J. Int.*, *161*, 861–880.

Slejko, D., L. Peruzza, and A. Rebez (1998), Seismic hazard maps of Italy, *Ann. Geofis.*, *41*(2), 183–214.

Stein, R. S. (2003), Earthquake conversations, *Sci. Am.*, *288*(1), 72–79.

Toda, S., D. Inoue, A. Kubouchi, N. Takase, and M. Nikaido (1995), Paleoseismicity of the Atera fault system and 1586 Tensho earthquake: trenching studies at Ogo, Aonohara and Dendahara, central Japan, *J. Seismol. Soc. Jpn.*, *48*, 401–421.

Valensise, G., and D. Pantosti (2001), The investigation of potential earthquake sources peninsular Italy: A review, *J. Seismol.*, *5*(3), 287–306.

Vezzani, L., and F. Ghisetti (1998), Carta Geologica Dell Abruzzo, 1:100000, SELCA SPA, Florence, Italy.

Vorobieva, I. A., and G. F. Panza (2004), Prediction of the occurrence of related strong earthquakes in Italy, *Pure Appl. Geophys.*, *141*(1), 25–41.

Walsh, J. J., J. Watterson, and G. Yielding (1991), The importance of small-scale faulting in regional extension, *Nature*, *351*, 391–393.

Walters, R. J., J. R. Elliott, N. D'Agostino, P. C. England, I. Hunstad, J. A. Jackson, B. Parsons, R. J. Phillips, and G. Roberts (2009), The 2009 L'Aquila Earthquake (central Italy): A source mechanism and implications for seismic hazard, *Geophys. Res. Lett.*, *36*, L17312, doi:10.1029/2009GL039337.

P. Cowie, Institute of Geography, School of Geosciences, University of Edinburgh, Drummond St., Edinburgh EH8 9XP, UK. (patience.cowie@glg.ed.ac.uk)

J. P. Faure Walker, G. Roberts, and P. Sammonds, Research School of Earth Sciences, UCL/Birkbeck, Gower St., London WC1E 6BT, UK. (j.p.faure.walker.02@cantab.net; gerald.roberts@ucl.ac.uk; p.sammonds@ucl.ac.uk)